國　立　交　通　大　學

電子工程學系電子研究所碩士班

碩　士　論　文

利用臨場共製的 ReFET 與 ISFET 來改善飄移特性之研究

The study of improving drift characteristics with co-fabricating ReFET and ISFET

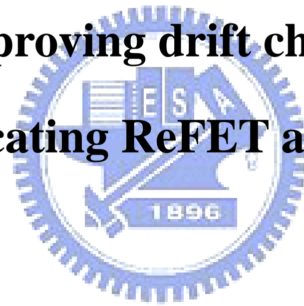

學生：吳冠增　　Student : Kuan-Tseng Wu

指導教授：張國明 博士　　Advisor : Dr. Kow-Ming Chang

桂正楣 博士　　Dr. Cheng-May Kwei

中華民國九十四年六月

利用臨場共製的 ReFET 與 ISFET 來改善飄移特性之研究

The study of improving drift characteristics with co-fabricating ReFET and ISFET

學生：吳冠增　　　　Student : Kuan-Tseng Wu

指導教授：張國明 博士　　　　Advisor : Dr. Kow-Ming Chang

桂正楣 博士　　　　Dr. Cheng-May Kwei

國立交通大學電子工程學系電子研究所碩士班

碩士論文

A Thesis
Submitted to Institute of Electronics
College of Electrical Engineering and Computer Science
National Chiao Tung University
In Partial Fulfillment of the Requirements
for the Degree of
Master of Science
In
Electronics Engineering

June 2005
Hsinchu, Taiwan, Republic of China

中華民國九十四年六月

利用臨場共製的 ReFET 與 ISFET 來改善飄移特性之研究

學生:吳冠增　　　　　　　　　　指導教授:張國明 博士

桂正楣 博士

國立交通大學

電子工程學系 電子研究所碩士班

摘要:

ISFET 最早是由 P.Bergveld 在 1970 年所提出的，其結構是將傳統的金氧半場效電晶體中的金屬閘極以待測溶液與參考電極所取代之。一旦待測溶液中的離子被感測層(sensing layer)表面的斷鍵所束縛住時，將會對下面的通道做出調變的效應，進而改變通道的電阻。如此一來，元件的電性將會隨著溶液的不同而產生變化，我們也同時藉由電性的變化來判定溶液的性質。

然而在我們的量測過程之中，輸出電壓的飄移效應是對元件穩定度影響最大的原因之一。如何去改善 ISFET 本身的飄移效應是目前所遇到的最大問題之一，這將會直接影響元件的使用壽命以及量測的準確度。不同的感測層，其本身的性質亦不盡相同。在本篇論文中，我們引入幾種與目前 CMOS 製程匹配的材料來做為感測層，結合適當的輸出電路的設計，以求可以將元件的飄移效應的影響降到最低。

實驗結果顯示，HfO_2-Si_3N_4對有最佳的飄移特性(0.19mv/hr)，可以大幅的減低飄移現象的影響。而在配合輸出電路後，TiO_2-ZrO_2對則有最佳的修正率(98%以上)。在最後並討論如何藉由本文的結果，在將飄移效應減至最低的前提之下，來適當的選取ReFET。

The study of improving drift characteristics with co-fabricating ReFET and ISFET

Student: Kuan-Tseng Wu

Advisor: Dr. Kow-Ming Chang

Dr. Cheng-May Kwei

Department of Electronics & Institute of Electronics

National Chiao Tung University

Abstract

The ion-sensitive field effect transistor (ISFET) was first introduced by P.Bergveld in 1970. The metal gate is replaced by a reference electrode and the electrolyte . Once the ions in electrolyte are trapped by the dangling bond at the surface of sensing layer , which will induce the modulation of channel resistance . Therefore, the electric characteristics are changed by different kinds of electrolyte , and we can distinguish the properties of electrolyte .

During measurement , the drift characteristics is a major problem for stability of device . That will directly affect the lifetime of device and accuracy of measurement . Depending on different sensing layers, the property of sensing layers varies . In this thesis , we use some kinds of CMOS-compatible materials as sensing layers combining output differential measurement circuit in order to reduce the drift effect .

According to our results , the S-HfO_2-Si_3N_4 pair has the best result of drift characteristic (0.19mv/hr after 10000 s) . And the TiO_2-ZrO_2 pair has the best of drift correction up to 98 % . At last , we will discuss that how to use the results here to choose proper ReFET in order to reduce the drift characteristics .

誌謝

一轉眼之間，二年的碩士生涯就要畫上一個句號。在電子所的這二年，我由衷地感謝張國明老師以及桂正楣老師的悉心教導，沒有他們的照顧，我無法如此順利地完成學業。除了研究上的指導之外，他們做人處世的態度，也讓我如沐春風。

此外要感謝的是趙高毅學長，在我的實驗過程中，不斷地給予我幫助以及建議，對於我的問題，他總是不厭其煩地教導我，讓我可以更順利地完成我的實驗。私底下，他也是一位對學弟相當照顧的學長。

而實驗室中融洽的氣氛，更凝聚了學長學弟之間的感情，也讓我在交大的二年有著無數的美好回憶。也感謝那些在實驗過程中一起共患難的學長學弟們，因為有你們的陪伴，即使在做實驗的深夜中，也不會感到任何的孤寂。

最後，也感謝我的家人，有她們的支持，我才無後顧之憂，可以全心衝刺完成我的學業。

Content

Abstract (in Chinese)……………………………………………………………..i

Abstract (in English)……………………………………………………………..ii

Acknowledgements (in Chinese)…………………………………………………..iii

Contents………………………………………………………………………….iv

Figure captions…………………………………………………………….….vi

Table captions…………………………………………………………………....ix

Chapter 1 Introduction

1.1 Overview of ISFET……………………………….……………….…………1

1.2 The characteristics of ISFET…………………………………………….……...2

1.3 The reasons of using ReFET…..…………………………..……………………3

1.4 The problems of ISFET system…………………………..………..………3

1.5 Thesis organization………………………………………………………………..4

1.6 References……………………………………………………………………4

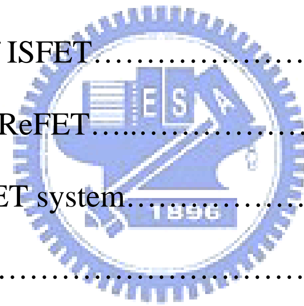

Chapter 2 Theory

2.1 General expression for the single sensing layer……………………………...6

2.1.1 The operational mechanism of ISFET……..…………………………....6

2.1.2 The pH sensitivity of ISFET……………………………………………7

2.2 The ReFET………………………………………..…………………….…...10

2.3 References……………………………………………………………………..12

Chapter 3 Experiment

3.1 Procedures of experiment..14

3.2 Experiment details..15

3.2.1 Gate region definition..15

3.2.2 Deposition of sensing layers..16

3.2.3 S / D contact area deposition..17

3.3 Measurement system 17

3.3.1 Electrical characteristics measurement..17

3.3.2 Differential sensing measurement..18

3.3.3 Drift measurement..18

3.4 References 19

1896

Chapter 4 Results and Discussions

4-1 Drift of different kinds of ISFET-ReFET pairs..20

4-2 To choose the proper ReFET..20

4-3 Conclusions..21

Chapter 5 Future Work

5-1 Future work..22

Figure Captions

Figure 1-1 Schematic representation of MOSFET (a) , ISFET (b) , and electronic diagram (c)

Figure 2-1 Potential profile and charge distribution at oxide / electrolyte interface

Figure 2-2 Differential measurement setup of an ISFET-ReFET pair

Figure 3-1 Experimental process

Figure 3-2 The system of measurement

Figure 4-1-a drift characteristic of sputter HfO_2 (sample-1)

Figure 4-1-b drift characteristic of LP-nitride (sample-1)

Figure 4-1-c drift characteristic of sample-1

Figure 4-2-a drift characteristic of E-gun HfO_2 (sample-2)

Figure 4-2-b drift characteristic of LP-nitride (sample-2)

Figure 4-2-c drift characteristic of sample-2

Figure 4-3-a drift characteristic of E-gun TiO_2 (sample-3)

Figure 4-3-b drift characteristic of LP-nitride (sample-3)

Figure 4-3-c drift characteristic of sample-3

Figure 4-4-a drift characteristic of E-gun Al_2O_3 (sample-4)

Figure 4-4-b drift characteristic of LP-nitride (sample-4)

Figure 4-4-c drift characteristic of sample-4

Figure 4-5-a drift characteristic of E-gun HfO_2 (sample-5)

Figure 4-5-b drift characteristic of Sputter HfO_2 (sample-5)

Figure 4-5-c drift characteristic of sample-5

Figure 4-6-a drift characteristic of E-gun HfO_2 (sample-6)

Figure 4-6-b drift characteristic of E-gun TiO_2 (sample-6)

Figure 4-6-c drift characteristic of sample-6

Figure 4-7-a drift characteristic of Sputter ZrO_2 (sample-7)

Figure 4-7-b drift characteristic of LP-nitride (sample-7)

Figure 4-7-c drift characteristic of sample-7

Figure 4-8-a drift characteristic of Sputter HfO_2 (sample-8)

Figure 4-8-b drift characteristic of Sputter ZrO_2 (sample-8)

Figure 4-8-c drift characteristic of sample-8

Figure 4-9-a drift characteristic of Sputter HfO_2 (sample-9)

Figure 4-9-b drift characteristic of E-gun Al_2O_3 (sample-9)

Figure 4-9-c drift characteristic of sample-9

Figure 4-10-a drift characteristic of E-gun TiO_2 (sample-10)

Figure 4-10-b drift characteristic of Sputter ZrO_2 (sample-10)

Figure 4-10-c drift characteristic of sample-10

Figure 4-11-a drift characteristic of E-gun TiO_2 (sample-11)

Figure 4-11-b drift characteristic of E-gun Al_2O_3 (sample-11)

Figure 4-11-c drift characteristic of sample-11

Figure 4-12-a drift characteristic of Sputter ZrO_2 (sample-12)

Figure 4-12-b drift characteristic of E-gun Al_2O_3 (sample-12)

Figure 4-12-c drift characteristic of sample-12

Table captions

Table 3-1 Specifications of wafers

Table 3-2-a Parameters of sensing layers deposition with E – gun

Table 3-2-b Parameters of sensing layers deposition with Sputter

Table 3-2-c Parameters of sensing layers deposition with LPCVD

Table 3-3 Recipe of HDP-RIE for LP-nitride

Table 4-1 Table of composition of ISFET – ReFET pairs

Table 4-2 The drift after 10000 s and the relative correction coefficient

Chapter 1

Introduction

1.1 Overview of ISFET

The first ion-sensitive field-effect transistor (ISFET) was reported by P. Bergveld in 1970 [1] . The ISFET can be considered as a special type of MOSFET without a metal gate , therefore the underlying insulator is directly exposed to the buffer solution . The schematic representation of a MOSFET and an ISFET is shown in Fig.1-1 .

At the beginning , in order to describe the operational mechanism of ISFET , P. Bergveld and A. Sibbald derived the general expression for the drain current of the ISFET in linear region .

Like in MOSFET , the channel resistance in ISFET depends on the electric field perpendicular to the direction of the current . Charges from solution accumulate on the top of this insulating membrane and do not pass through the ion-sensitive membrane . The dependence of the interfacial potential on the charge concentration can be explained with the well-known site-binding theory . In 1974 , Yates et al [2] introduced the site-binding model in colloid chemistry to describe the properties of an oxide-aqueous electrolyte interface . In this model , the oxide surfaces are assumed to be amphoteric , meaning that the surface hydroxyl groups can be neutral , protonized (positively charged) or deprotonized (negatively charged) depending on the pH of the electrolyte . This model was later adapted to describe the insulator-electrolyte interface of an ISFET .

This basic model was adopted to the electrolyte/insulator/silicon (EIS) structure

by Bousse [3], a Ph.D student of P. Bergveld in 1980 , and proved to be applicable for ISFET surfaces of SiO_2 and Al_2O_3 . Bousse developed a simple theory with two parameters which is derived from the site-dissociation and double-layer models . One of the parameters is the pH_{pzc} , being the value of the pH for which the oxide surface is electrically neutral , and the other is β . The value of β can be expressed in terms of the acidic and basic equilibrium constants of the related surface reactions , for which a parameter $[H^+]_s$ has been introduced , which represents the surface concentration of H^+ ions , being related to the $[H^+]$ bulk value by Boltzmann statistics .

At present , the model presented by Bousse [4] is accepted as a good description for the ISFET response commonly but a description of the sensitivity that can be interpreted easily . Additionally , the model is not valid over the entire pH range and neglects the influences of ionic strength .

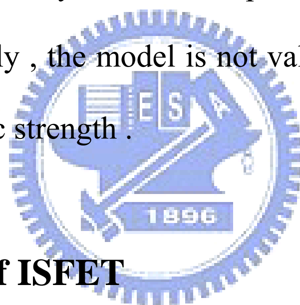

1.2 The characteristics of ISFET

The sensing layer is the most significant part in ISFET . A change of the pH concentration in the electrolyte will result in a change of the surface potential between electrolyte and insulator , which will induce the alteration of the electric field in the insulator-semiconductor interface and the modulation of the channel conductance and current .

In the past , various dielectrics , e.g. SiO_2 [1] , Si_3N_4 [5,6] , Al_2O_3 [7,8] , Ta_2O_5 [9,10] , WO_3 [11] , and SnO_2 [12,13] , were investigated as pH-sensitive gate insulator materials . The ISFET sensing properties are greatly dependent upon various materials owing to the different electrolyte reactivity with these materials . Initially , SiO_2 was used as sensing membrane of ISFET , but the sensitivity and response of

that is unsatisfactory . Afterward , Si_3N_4 , Ta_2O_5 , and Al_2O_3 were used as gate dielectric because of higher dynamic response . Besides , as the time of operating increases , the drift characteristic of ISFET is also a major problem that we can not ignore .

1.3 The reasons of using ReFET

The reference ion-sensitive field-effect transistor (ReFET) is nothing but another ISFET which is less-sensitive . The ideal ReFET for a pH sensor would be completely insensitive to hydrogen ions but identical to the ISFET in terms of transconductance , thermal response , etc [14] . This can be achieved by coating an ISFET with a polymer membrane to prevent the hydrogen ions from reaching the insulator surface . In the thesis , we choose some CMOS-compatible oxides to fabricate ReFETs . After combining the differential measurement setup with the ISFET-ReFET pair , some non-ideal effects , such as drift characteristic and temperature effect , can be alleviated .

1.4 The problems of ISFET system

The ion-sensitive field-effect transistors (ISFETs) have potential advantages to conventional to ion selective electrode (ISE) in their small size , rapid response , low output impedance , low cost and so on [15-17] . These properties make ISFET have great prospective utility in the field of chemical analysis , biomedicine research , and industrial manufacture and monitoring .

In practical application of ISFET , a standard reference electrode is required to provide a reference electric potential . However , the size of the standard reference

electrode is relative big , it is not suitable for applications , especially when the sample is little .

1.5 Thesis organization

At first , we briefly introduce the history and properties of ISFET and the reasons of using ReFET in chapter 1 . In the next chapter , the operation mechanism of ISFET and ReFET is discussed . The entire experiment procedures and measurement setup details are described in chapter 3. In this chapter , the different kinds of ISFET-ReFET pair is fabricated . After measuring the characteristics of the devices, we bring up some ideas about the results and show the conclusions in chapter 4. At last, some works are presented to do in the future.

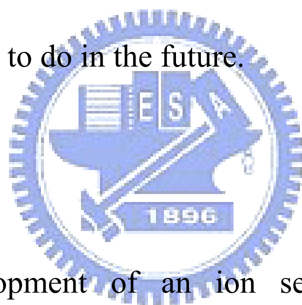

1.6 References

[1] P. Bergveld , " Development of an ion sensitive solid-state device for neurophysiological measurements" , IEEE Trans.Biomed. Eng.,vol. BME-17 (1970) p.70

[2] D.E. Yates , S. Levine and T.W. Healy , "Site-binding model of the electrical double layer at the oxide/wafer interface " , J. Chem. Soc. Faraday Trans. , 70 (1974) p.1807-1818

[3] L.J. Bousse , N.F. de Rooij , P. Bergveld , "Operation of chemically sensitive field effect sensors , as function of the properties of the insulator/electrolyte interface " , IEEE Trans. Electron Devices ED-30 (1983) p.1263-1270

[4] L. Bousse , Ph.D. Thesis , Technische Hogeschool Enschede , The Netherlands (1982)

[5] L. Bousse , D. Hafeman , N. Tran , Sens. Actuators B1 (1990) p.361

[6] K.M. Chen , G.H. Li , L.X. Chen , Y. Zhu , Sens. Actuators B13-B14 (1993) p.209

[7] T. Matsuo , M. Esashi , H. Abe , IEEE Trans. Electron Devices 26-11 (1979) p.1856

[8] W. Moritz , B.H. van der schoot , N.F. de Rooij , H.H. van den Vlekkert , H.G. Ligtenberg , Sens. Actuators B13-B14 (1993) p.217

[9] M. Klein , M. Kuisl , VDI-Berichte 509 (1984) p.275 (German)

[10] A.S. Poghossian , Sens. Actuators B7 (1992) p.367

[11] J.C. Chou , J.L. Chiang , Sens. Actuators B62 (2000) p.81

[12] L.L. Chi , J.C. Chou , W.Y. Chung , T.P. Sun , S.K. Hsiung , Mater. Chem. Phys. 63 (2000) p.19

[13] H.K. Liao , L.L. Chi , J.C. Chou , W.Y. Chung , T.P. Sun , S.K. Hsiung , Mater. Chem. Phys. 59 (1999) p.6

[14] Paul A. Hammond , Danish Ali , and David R. S. Cumming , " Design of a Single-Chip pH Sensor Using a Conventional 0.6-μm CMOS Process " , IEEE Sensors Journal , vol. 4 , No. 6 December (2004)

[15] A. Merlos , E. Cabruja , J. Esteve , Sens. Actuators B24/25 (1995) p.228

[16] T. Matsuo , M. Esashi , Sens. Actuators 1 (1981) p.77

[17] J. Bausells , J. Carrabina , A. Errachid , A. Merlos , Sens. Actuators B57 (1999) p.56

Chapter 2

Theory

2.1 General expression for the single sensing layer

2.1.1 The operational mechanism of ISFET

The ISFET is in fact nothing else than a MOSFET with the gate connection separated from the chip in the form of a reference electrode inserted in an aqueous solution which is in contact with the gate oxide .

The general expression for the drain current of the MOSFET and thus also of the ISFET in the non-saturated mode is

$$Id = C_{ox}\,\mu\,\frac{W}{L}\left[\,(Vgs - Vt)\,Vds - \frac{1}{2}Vds^2\,\right] \qquad \text{.............................(1)}$$

where C_{ox} is the oxide capacity per unit area ; W and L are the width and the length of the channel , respectively ; Vgs and Vds are the gate source voltage and the drain source voltage . And the μ is the electron mobility in the channel .

In case of the ISFET , the expression of threshold voltage becomes

$$Vt = E_{ref} - \Psi_o + \chi^{sol} - \frac{\Phi_{Si}}{q} - \frac{Q_{OX}+Q_{SS}+Q_B}{C_{OX}} + 2\,\phi_f$$

where E_{ref} is the constant potential of the reference electrode , and the interfacial potential $\Psi_o + \chi^{sol}$ at the solution/oxide interface of which Ψ_o is the chemical input parameter , shown to be a function of the solution pH and χ^{sol} is the surface dipole potential of the solvent and thus having a constant value ; Φ_{Si} is the silicon work function ; q is the elementary charge ; Q_{OX} , Q_{SS} , Q_B are the charges located in the oxide , charges located at the oxide-silicon interface , and the depletion charges in the silicon respectively . And the ϕ_f is the potential difference between the Fermi levels

of doped and intrinsic silicon .

The general expression for the drain current of the ISFET in the non-saturated region described by P. Bergveld and A. Sibbald [1] is

$$Id = C_{ox}\,\mu \frac{W}{L} \{ [Vgs - (E_{ref} - \Psi_o + \chi^{sol} - \frac{\Phi_{Si}}{q} - \frac{Q_{OX}+Q_{SS}+Q_B}{C_{OX}} + 2\,\phi_f)]\, Vds - \frac{1}{2} Vds^2 \}$$

All parameters are constant except the electrostatic potential at the surface Ψ_o and the surface dipole potential χ^{sol} . The surface dipole potential is supposed to be independent of pH and changes in the drain current are therefore attributed to changes in the electrostatic potential , Ψ_o , only .

2.1.2 The pH sensitivity of ISFET

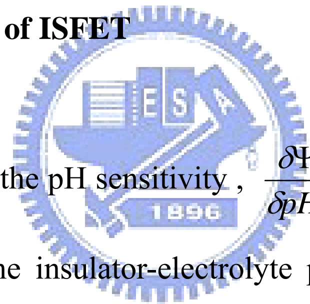

A general expression for the pH sensitivity , $\frac{\delta \Psi_0}{\delta pH_B}$, which is the change of the bulk pH over a change of the insulator-electrolyte potential , Ψ_o , is given . The expression is derived from a separate treatment of both sides of the double layer (gate insulator and the electrolyte) . The site-dissocuation model introduced by Yates et al [2] in 1974 describes the charging mechanism of an oxide as the result of an equilibrium between the AOH surface sites and the H^+ ions in the bulk of the solution . The surface reaction are [2] :

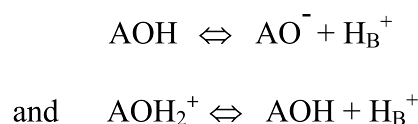

$$AOH \Leftrightarrow AO^- + H_B^+$$

and $$AOH_2^+ \Leftrightarrow AOH + H_B^+$$

where B refers to the bulk .

with the following thermodynamic equations :

$$\mu^o_{AOH} + kT \ln \nu_{AOH} = \mu^o_{AO^-} + kT \ln \nu_{AO^-} + \mu^o_{Hs^+} + kT \ln a_{Hs^+} \qquad \text{...........(2)}$$

and

$$\mu^{o}_{AOH_2^+} + kT \ln \nu_{AOH2^+} = \mu^{o}_{AOH} + kT \ln \nu_{AOH} + \mu^{o}_{Hs^+} + kT \ln a_{Hs^+} \quad \text{............(3)}$$

where ν_i is the surface activity and μ^{o}_{i} is the standard chemical potential of species i .

Equation (2) and (3) can be rearranged to :

$$\frac{\nu_{AO^-} \cdot \alpha_{HS^+}}{\nu_{AOH}} = K_a \quad \text{with} \quad K_a = \exp\frac{\mu^0_{AOH_2^+} - \mu^0_{AO^-} - \mu^0_{H_B^+}}{kT}$$

and

$$\frac{\nu_{AOH} \cdot \alpha_{HS^+}}{\nu_{AOH_2^+}} = K_b \quad \text{with} \quad K_b = \exp\frac{\mu^0_{AOH_2^+} - \mu^0_{AOH} - \mu^0_{H_B^+}}{kT}$$

where the K_i values are dimensionless intrinsic dissociation constants ; ν_i is the number of sites per unit area . The relationship between the surface activity of H^+ , α_{HS^+} , and the bulk activity of H^+ , α_{HB^+} , is given by the Nernst equation [3]:

$$a_{Hs^+} = a_{HB^+} \exp\frac{-q\Psi_0}{\kappa T}$$

$$\text{or} \quad pH_s = pH_B + \frac{q\Psi_0}{2.3\kappa T} \quad \text{..................................(4)}$$

where q is the elementary charge , k is the Boltzmann constant and T is the absolute temperature . The surface charge density , σ_0 , is given by

$$\sigma_0 = q\,(\nu_{AOH2^+} - \nu_{AO^-}) = q\,N_s\,(\Theta^+ - \Theta^-) \quad \text{..................................(5)}$$

where N_s is the density of the available sites ; Θ^+ and Θ^- are the fractions of N_s carrying charge , i.e. , AOH_2^+ and AO^- , respectively . The fractions Θ^+ and Θ^- are calculated from the Eq. (2) and Eq. (3) and substitutes in Eq. (5) to give

$$\sigma_0 = q \cdot N_s \cdot \frac{a^2_{HS^+} - K_a \cdot K_b}{K_a \cdot K_b + K_b \cdot a_{HS^+} + a^2_{HS^+}} = -q\,[B] \quad \text{......................(6)}$$

where [B] is the number of negatively charged groups minus the number of positively charged groups per unit area . pH_{pzc} , pH at the point of zero charge , is defined as the pH were both fractions are equal and [B] is zero . The change in the number of charged groups as a result of an infinitesimal increase in pH_s is the intrinsic buffer capacity , β_{int} :

$$\frac{\delta\sigma_0}{\delta pH_s} = -q \cdot \frac{\delta[B]}{\delta pH_s}$$

$$= -q \cdot N_s \cdot \frac{K_b \cdot a^2{}_{HS^+} + 4 \cdot K_a \cdot K_b \cdot a_{HS^+} + K_a \cdot K_b{}^2}{K_a \cdot K_b + K_b \cdot a_{HS^+} + a^2{}_{HS^+}} \cdot 2.3\, a_{Hs^+}$$

$$= -q \cdot \beta_{int} \quad \ldots\ldots\ldots\ldots\ldots\ldots\ldots\ldots\ldots\ldots\ldots\ldots\ldots(7)$$

the charge in the electrolyte is equal but opposite to the charge on the oxide surface . The Gouy-Chapman-Stern model is used to describe the electrolyte side of the double layer . This model involves a diffuse layer of charge in the solution starting at a distance X_2 from the surface . This distance X_2 is the plane of closest approach for the center of the ions in the solution (Stern layer) . The charge in the diffuse layer is [4] (Fig. 2-1)

$$\sigma_{DL} = -(8kT\varepsilon\varepsilon_0 n^0)^{\frac{1}{2}} \cdot \sinh(\frac{zq\phi_2}{2kT}) = -Ci\,\Psi_o = -\sigma_0 \quad \ldots\ldots\ldots\ldots\ldots(8)$$

where ε_0 is the permittivity of free space and ε is the relative permittivity ; Φ_2 is the potential at X_2 ; n^o is the number concentration of each ion in the bulk and z is the magnitude of the charge on the ions . the integral capacitance , Ci , is often denoted as K . The ability of the electrolyte to store charge in response to a change in the electrostatic potential is the differential capacitance [4]

$$\frac{\delta\sigma_{DL}}{\delta\Psi_0} = -\frac{\delta\sigma_0}{\delta\Psi_0}$$

$$= - \frac{\left(\frac{2\varepsilon\varepsilon_0 z^2 q^2 n^0}{kT}\right)^{\frac{1}{2}} \cosh(\frac{zq\phi_2}{2kT})}{1+\left(\frac{X_2}{\varepsilon\varepsilon_0}\right)\left(\frac{2\varepsilon\varepsilon_0 z^2 q^2 n^0}{kT}\right)^{\frac{1}{2}} \cosh\left(\frac{zq\phi_2}{2kT}\right)}$$

$$= - C_{dif} \quad \text{..(9)}$$

combination of both sides of the double layer (Eqs. (7) and (9)) yields

$$\frac{\delta\Psi_0}{\delta pH_s} = \frac{\delta\Psi_0}{\delta\sigma_0}\frac{\delta\sigma_0}{\delta pH_s} = \frac{-q\beta_{int}}{C_{dif}} \quad \text{...(10)}$$

the relation between pH_s and pH_B is given by the Nernst equation (Eq.(4)) . Substitution of Eq.(4) in Eq.(10) and rearrangement gives the general expression for the sensitivity of the electrostatic potential to changes in the bulk pH :

$$\frac{\delta\Psi_0}{\delta pH_B} = - 2.3\frac{kT}{q}\alpha \quad \text{...(11)}$$

$$\text{with } \alpha = \frac{1}{\frac{2.3kTC_{dif}}{q^2\beta_{int}}+1}$$

where α is a dimensionless sensitivity parameter . The value of α varies between 0 and 1 depending on the intrinsic buffer capacity and the differential capacitance . The site-binding theory and the Gouy-Chapman-Stern model were used in the derivation of this model , but other theories can be used as well to determine the intrinsic buffer capacity [5] , the differential capacitance and thus the sensitivity parameter α .

2.2 The ReFET

A pH reference field effect transistor (pH-ReFET) is just an ISEFT , which is less sensitive to pH . Most of the attempts to creat a ReFET are based on covering the gate oxide of an ISFET with an additional ion insensitive membrane .

Several ReFETs have been made based on different approaches , such as using a

buffered hydrogel as insensitive membrane [6] or with an ion-blocking parylene gate [7] . The first publication concerning this approach is from Matsuo , who deposited a parylene film on the Si_3N_4 gate of an ISFET [8] . Although the goal to make pH sensitivity decrease as possible is obtained , the stability of FET was not as expected , probably due to its pinholes on this very thin layer . Once time of measurement increases , the characteristic of ReFET will gradually get worse because of the trapping charges in the film and the loss of the ability to isolate H^+ from oxide beneath . Therefore , other membranes have also been deposited , usually thicker layers , such as Teflon [9] .

Recently , PVC membrane is another choice , especially in chemical detection and analysis [10,11] . However , there are still some problems about the utility of PVC membrane . The PVC has usually not been considered for ReFETs as it typically shows cation permselectivity [12] . This behavior is common to many polymeric membranes , and means that the membranes are permeable for cations . That will affect dramatically the electrical characteristic and the stability of ISFET because of the directly contact between sensing film and electrolyte to be analyzed .

In the thesis , we develop a ReFET which can be fabricated with ISFET at the same time . To measure ISFET-ReFET pairs , a differential measurement setup shown in Fig. 2-2 to maintain both I_{DS} and V_{DS} constant is taken into our experiment . The upper current source forces a constant current I_{DS} through the ISFET , while the lower current sinker forces an identical current through the fixed resistor R_{DS} to give a constant voltage drop . The qRE we implement here is a conventional reference electrode . Under the condition of both I_{DS} and V_{DS} are given constant , and according to Eq. (1) , V_G is varies with the change of threshold voltage , V_T , which depends on the pH value of electrolyte that we analyze . For an ideal ReFET , V_T does not vary and so $V_{G(RE)}$ is constant ; the difference , ($V_{G(IS)} - V_{G(RE)}$) , forms the pH-dependent

signal .

2.3 Reference

[1] P. Bergveld and A. Sibbald , " Analytical and Biomedical Applications of ISFETs " , Elsevier , Amsterdam , (1988)

[2] D.E. Yates , S. Levine and T.W. Healy , " Site-binding model of the electrical double layer at the oxide/wafer interface " , J. Chem. Soc. Faraday Trans. , 70 (1974) p.1807-1818

[3] P. Bergveld , " Development of an ion-sensitive solid-state device for neuro-physiological measurements " , IEEE Trans. Biomed. Eng. , BME-17 (1970) p.70.

[4] A.J. Bard and L.R. Faulkner , " Electrochemical Methods Fundamentals and Applications " , Wiley , New York , (1980)

[5] T. Hiemstra , W.H. van Riemsdijk and G.H. Bolt , " Multisite proton adsorption modeling at the solid/solution interface of (hydr)oxides : a new approach " , J. Colloid Interface Sci , 133 (1989) p.91-104

[6] P. A. Comte , J. Janata , " A field-effect transistor as a solid-state reference electrode " , Anal. Chim. Acta 101 (1978) p.247-252

[7] T. Matsuo , H. Nakajima , " Characteristics of reference electrodes using a polymer gate ISFET " , Sens. Actuators 5 (1984) p.293-305

[8] T. Matsuo , M. Esashi , in : Proceedings of the 153rd Meeting of the Electro-chemical Society Extended Abstract (1978) p.202-203

[9] H. Nakajima , M. Esashi , T. Matsuo , " The cation concentration response of polymer gate ISFET " , J. Electrochem . Soc. 129 (1982) p.141-143

[10] M. J. Madou , S. R. Morrison , Chemical Sensing with Solid State Devices , Academic Press , San Diego , CA , USA , (1989)

[11] A. Errachid , J. Bausells , N. Jaffrezic-Renault , " A Simple REFET for pH detection in differential mode " , Sens. Actuator B60 (1999) p.43-48

[12] A. van den Berg , " Ion sensors based on ISFET's with synthetic ionophores " , ph.D Thesis , Univ. of Twente , the Netherlands , (1988)

Chapter 3

Experiment

3.1 Procedures of experiment

All procedures of experiment are done in NDL (National Nano Device Laboratory) and NFC (Nano Facility center) . The corresponding crosssection graph is illustrated in Fig . 3-1 .

1. RCA clean .
2. Wet oxidation 6000 Å .

   Temperature = 1050℃ for 65 min .

3. Mask - Ⅰ. S / D definition .
4. BOE etch wet oxide .
5. Dry oxidation for screening 300 Å .

   Temperature = 1050℃ for 12 min .

6. S / D implantation .

   5e15 ($1/cm^2$)，25Kev (P)

7. N-type annealing .

   Temperature = 950℃ for 30 min .

8. PECVD - oxide for 1 μm .
9. Mask - Ⅱ. contact hole & gate region definiton .
10. BOE etch PECVD - oxide for 1 μm (contact hole region) .

    PECVD - oxide for 1 μm+ wet oxide for 6000 Å (gate region) .

11. Dry oxidation 100 Å (gate oxide) .

Temperature = 850℃ for 60 min .

12. Sensing layer α deposition .

13. Mask - Ⅲ. sensing layer α definition .

14. Etch of sensing layer α .

15. Sensing layer β deposition .

16. Mask - Ⅳ. sensing layer β definition .

17. Etch of sensing layer β .

18. Annealing in pure O_2 .

Temperature = 850℃ for 60 min .

19. Deposition of Ti / Pt .

20. Mask - Ⅴ. Ti / Pt region definition .

21. Pt annealing .

Temperature = 400℃ for 30 min .

22. Thermal coating of Al (back side) 5000 Å .

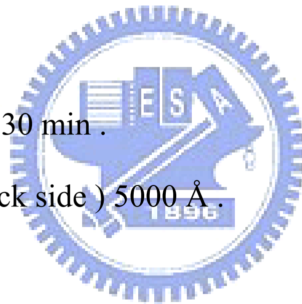

3.2 Experiment details

3.2.1 Gate region definition

First of all , in order to remove particles、metal ions and native oxide , RCA clean must be done in our experiment . P-type wafers were purchased from CARTINA (Table. 3-1) . Then we deposit wet oxide (6000 Å) for the define of S/D region . The oxide is also used for blocking layer during S/D implantation . The density and the energy of S/D implant is 5E15 (1/cm^2) and 25 KeV in phosphorous . After implantation , N-type annealing is required for activating the dopants . That is done at 950℃ for 30 min .

In standard MOSFET process, we do not have to deposit oxide for 1 μm by PECVD , however , it is necessary for protecting structure in using as a pH-ISFET [1] . During our measurements , the sensing region is immersed in electrolyte for a long time . The ions in electrolyte may diffuse into structure of ISFET and influence the electric characteristics . So we must deposit a thick passivation layer to avoid the influences of electrolyte [2] . Following above , we grow dry oxide for 100 Å as gate oxide after etch of PE-oxide . This layer is not only the critical structure which is significant for the electric characteristics of FET but also the key of improving adhesion toward our sensing layers .

3.2.2 Deposition of sensing layers

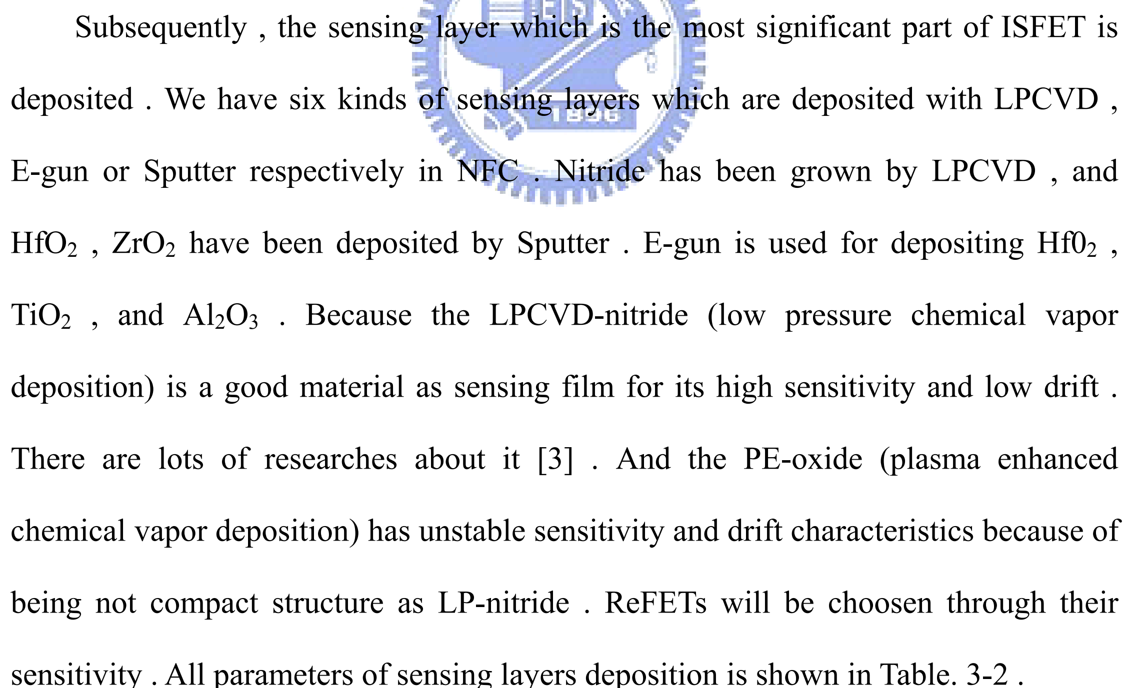

Subsequently , the sensing layer which is the most significant part of ISFET is deposited . We have six kinds of sensing layers which are deposited with LPCVD , E-gun or Sputter respectively in NFC . Nitride has been grown by LPCVD , and HfO_2 , ZrO_2 have been deposited by Sputter . E-gun is used for depositing $Hf0_2$, TiO_2 , and Al_2O_3 . Because the LPCVD-nitride (low pressure chemical vapor deposition) is a good material as sensing film for its high sensitivity and low drift . There are lots of researches about it [3] . And the PE-oxide (plasma enhanced chemical vapor deposition) has unstable sensitivity and drift characteristics because of being not compact structure as LP-nitride . ReFETs will be choosen through their sensitivity . All parameters of sensing layers deposition is shown in Table. 3-2 .

In this thesis , ISFET-ReFET pairs have been combined with external differential measurement setup , and that will accomplish the goal of improving long-term drift and stability .

3.2.3 S / D contact area deposition

Following sensing layer deposition , LP-nitride layer is etched by HDP-RIE (High Density Plasma Reactive Ion Etch) (Table. 3-3). And the etch of the other sensing films in our experiment is done by 49 % HF .

In deposition of S/D contact area , Pt layer of 1000 Å is chosen . However , adhesion between Pt and silicon is very bad. Ti is a good adhesion layer between silicon and Pt . So the double layer of Ti/Pt is formed by E-gun [4]. At last , 150ml HNO_3, 450ml HCl and 600ml water are mixed for the wet etching of Pt . Finally , Al is deposited on the backside of the silicon by thermal coater .

3.3 Measurement system

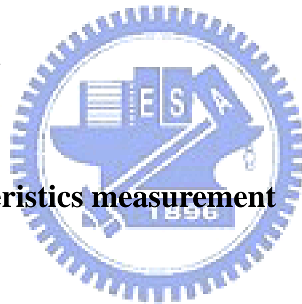

3.3.1 Electrical characteristics measurement

In our experiment , HP-4156 is used to measure the electrical characteristics of the ISFETs . The system of measurement is shown in Fig. 3-2 . All the measurements must be done in the dark box at 25 ℃ , because of the influences of light [5] . In the setup of HP-4156 , substrate is grounded and the reference electrode is sweeping to different voltages .

Before measurement , we have to glue a plastic container right on the top of the sensing area which must contact with buffer solution . In the plastic container , we add the buffer solutions with different pH values with the dropper . At first , adding buffer solution of pH 7 for several minutes is to balance the interface potential between electrolyte and oxide . The pH buffer solutions that we use are purchased from Riedel-deHaen and the pH-value is 1 , 3 , 5 , 7 , 9 , 11 , 13 respectively .

Because the electric potential of the pH-solution is always floating [6] , the disturbance from the surroundings would induce the electric potential variance of the solution . A reference electrode must be inserted into the electrolyte for provide a constant potential . An ideal reference electrode for use as the ISFET gate terminal should provide [7] :

1) an electrical contact to the solution from which to define the solution potential .
2) an electrode / solution potential difference that does not vary with solution composition .

3.3.2 Differential sensing measurement

We use external circuit to make a differential potentiometric measurement with an instrumentation amplifier between the ISFET and the ReFET , which are both oxide-based FETs and electrically identically devices [8] . In our experiment , we still make differential sensing with a conventional electrode (qRE) to provide a constant potential . Since both ISFET and ReFET operate under the same conditions , changes in temperature and solution potential will affect both equally and then the non-ideal influences of ISFET can be alleviated . Between measurement with next one , in order to reach the accuracy of measurement, the container has to be washed by the next pH-solution after measuring previous pH value.

3.3.3 Drift measurement

On measurement of drift characteristic , Id-Vg curves at pH 7 will be extracted for every particular period we set in stress program . Then under the condition of

constant Id , we plot the diagram of Vg versus time . Drift characteristic of ISFET changes fast initially and then keeps stable several hours later . Using differential measurement of ISFET-ReFET pair , the goal to reduce this non-ideal effect can be obtained . Total measurement time is 25870 seconds and Vg depends on the Id current that we keep constant .

3.4 References

[1] U. Guth , " Investigation of corrosion phenomena on chemical microsensors " , Electrochimica Acta 47 (2001) p.201-210

[2] George T. Yu , " Hydrogen ion diffusion coefficient of silicon nitride thin films " , Applied Surface Science 202 (2002) p.68-72

[3] P. Hein , " Drift behavior on ISFET with nitride gate insulator " , Sensors and Actuators B , 13-14 (1993) p.655-656

[4] I-Yu Huang , " Fabrication and characterization of a new planar solid-state reference electrode for ISFET sensors " , Thin Solid Films 406 (2002) p.255-261

[5] Hung-Kwei Liao , " Multi-structure ion sensitive field effect transistor with a metal light shield " , Sensors and Actuators B61 (1999) p.1-5

[6] P. Bergveld , " How electrical and chemical requirements for REFETs may coincide " , Sensors and Actuators 18 (1999) p.309-327

[7] Paul A. Hammond , Danish Ali , and David R. S. Cumming , " Design of a Single-Chip pH Sensor Using a Conventional 0.6-µm CMOS Process " , IEEE Sensors Journal , vol. 4 , No. 6 December (2004)

[8] P. A. Hammond , D. R. S. Cumming , D. Ali , " A Single-Chip pH Sensor Fabricated by a Conventional CMOS Process " , IEEE (1991)

Chapter 4

Results and Discussions

4-1 Drift of different kinds of ISFET-ReFET pairs

In our work , we choose five kinds of CMOS-compatible materials which are silicon nitride (Si_3N_4) 、 Hafnium oxide (HfO_2) 、 Titanium oxide (TiO_2) 、 Zirconium oxide (ZrO_2) 、 and Aluminium oxide (Al_2O_3) as sensing layers of ISFET . Sputter and E-gun are used for deposition of HfO_2 film . So we have twelve kinds of ISFET-ReFET pairs for demonstrate the drift characteristics of sensing layers we choose here . Table. 4-1 shows the composition of ISFET-ReFET pairs . In different kind of ISFET-ReFET pair , we keep Id constant respectively . The drift characteristics curves of every kind of ISFET-ReFET pairs in our work are shown in Fig. 4-1 ~ Fig. 4-12 . The relative drift after ten thousand seconds and the correction coefficient are listed in Table. 4-2 .

We can find that the drifts of silicon nitride film and E-gun HfO_2 film are very unstable . But we can correct the shortcomings by using differential measurement setup . The correction coefficient means that the drift improving percentage after ten thousand seconds . If the ISFET-ReFET pair has compatible drift characteristics , the result of improving drift characteristics is remarkable .

4-2 To choose the proper ReFET

According to our results about ISFET-ReFET pairs , we can obtain the drift characteristics of every kind of sensing films we choose . First , we must choose a sensing layer of ReFET that has similar drift characteristics with the sensing layer of ISFET we used here . Because the ISEFT-ReFET pair has compatible drift

characteristics , we can obtain better result of improving drift characteristics . And then we take the sensitivities of sensing layers into consideration in order to define ReFET . Even if the sensitivity of ISFET-ReFET pair is not quite high after differential measurement , we still can distinguish the voltage difference due to different pH value of buffer solution .

4-3 Conclusions

In sample-1 、sample-10 and sample-11 , the correction coefficient is quite high because of the compatibility of drift characteristics of two kinds of sensing layers . That is to say we can obtain a great improvement of drift characteristics . If the difference of drift between two kinds of sensing layers is large , the result of improving drift is limited (sample-3 、sample-5 and sample-12) . Once the difference of drift between two kinds of sensing layers is quite large , we even may not obtain any improvement (sample-4 and sample-7) . According to our results about drift , we can choose the most appropriate ReFET that has the most compatible drift characteristics with ISFET we use here and even predict the effect of drift to sensitivity of ISFET-ReFET pair . Once the drift characteristics can be reduced as possible , the stability of ISFET-ReFET pair will get better naturally to solving a major problem of ISFET .

According to our results , the S-HfO_2-Si_3N_4 pair has the best result of drift characteristic (0.19mv/hr after 10000 s) . And the TiO_2-ZrO_2 pair has the best of drift correction up to 98 % .

Chapter 5

Future Work

5-1 Future work

According to our results , we can have a data base to choose proper ReFET for the ISFET we used . We can find that some kind of ISFET-ReFET pair has great improvement to drift characteristics . In order to realize miniaturization , we can integrate reference electrode with ISFET-ReFET pair on the same chip in the future . Combining with MEMS technology , we also can fabricate a multi-channel sensor for sensing different kinds of materials at the same chip .

Besides , the external differential measurement circuit is a subject that we have to study in the future . Even we can focus on compensation of the non-ideal effect at the same time .

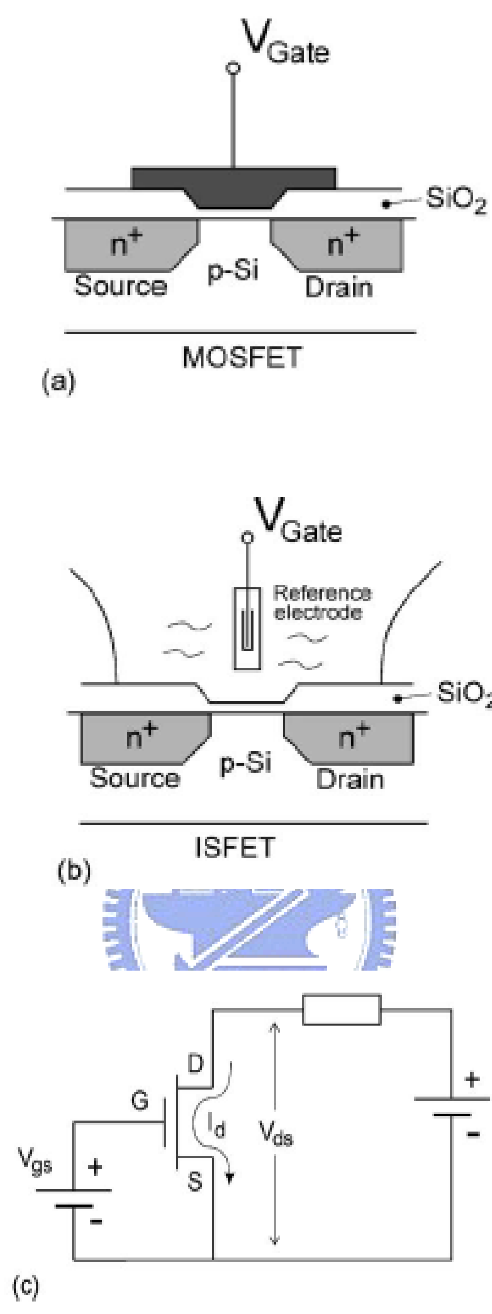

Figure 1-1 Schematic representation of MOSFET (a) , ISFET (b) , and electronic diagram (c) .

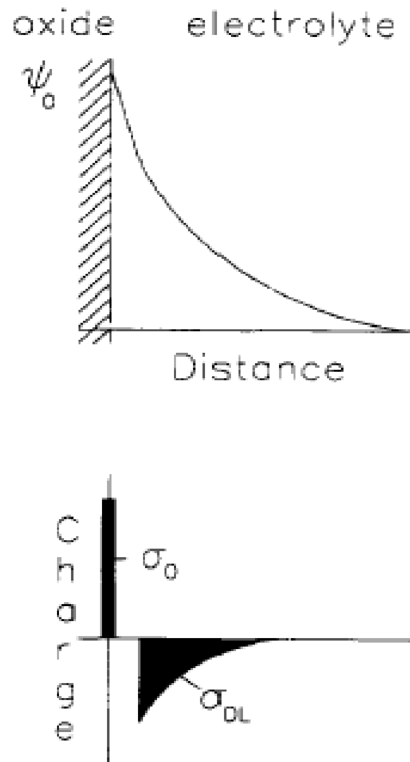

Figure 2-1 Potential profile and charge distribution at oxide / electrolyte interface

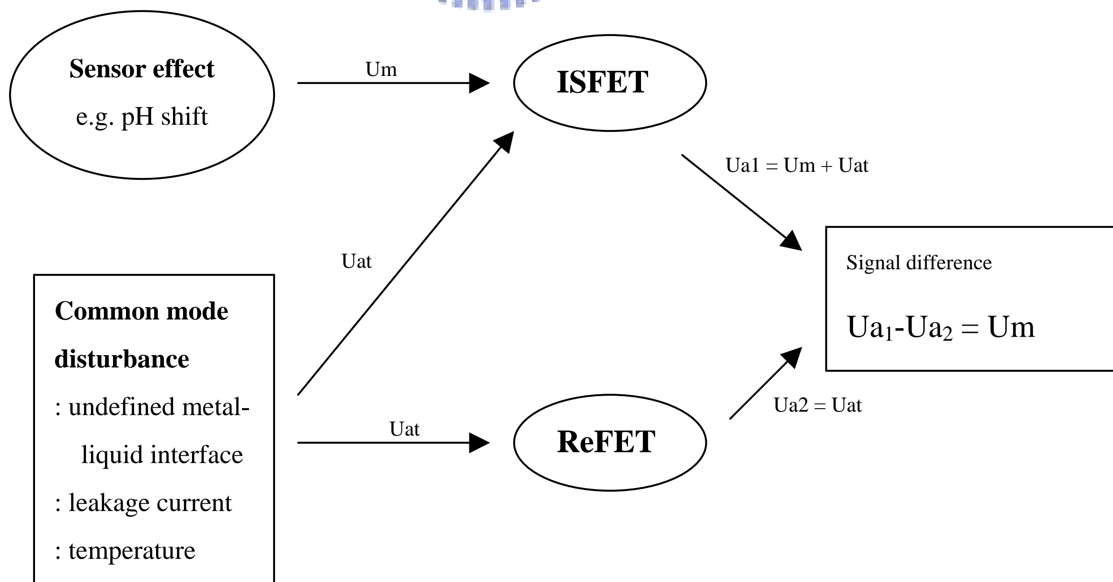

Figure 2-2 Differential measurement setup of an ISFET-ReFET pair

`

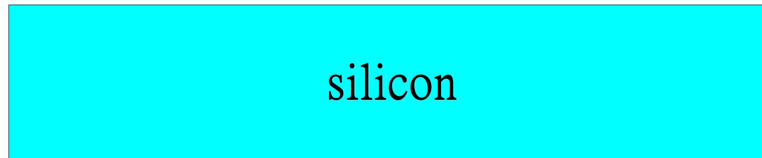

(a) RCA clean bare silicon

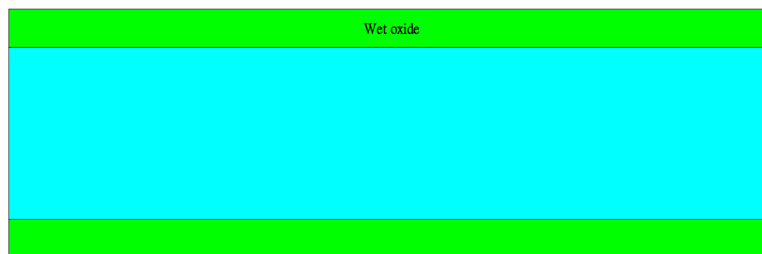

(b) wet oxidation

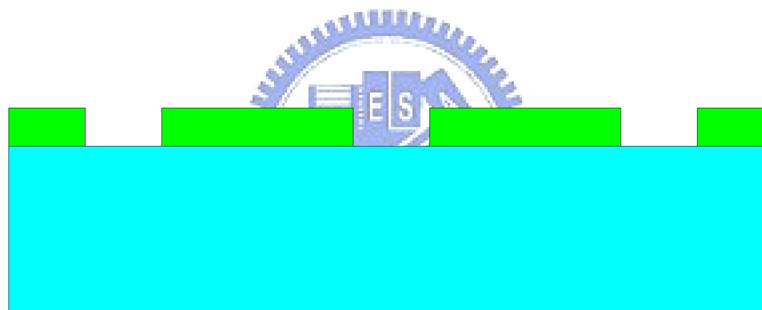

(c) mask Ⅰ

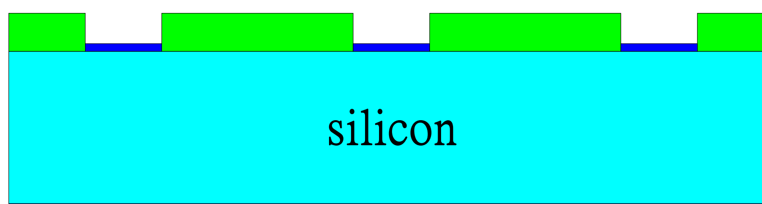

(d) screening oxidation

Figure 3-1 Experimental process

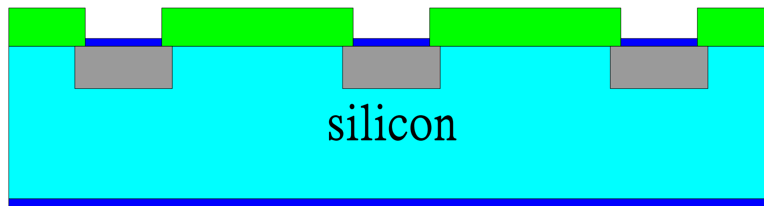

(e) implantation

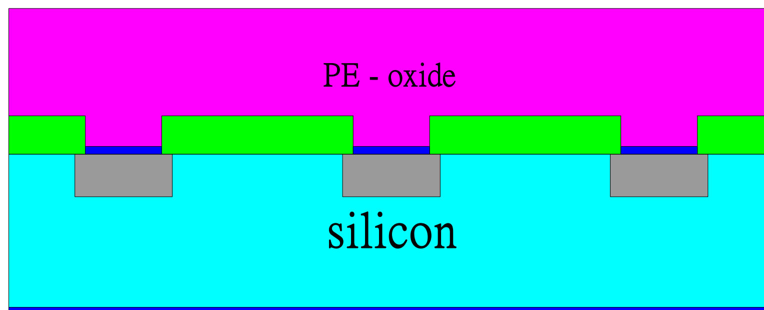

(f) passivation layer deposition

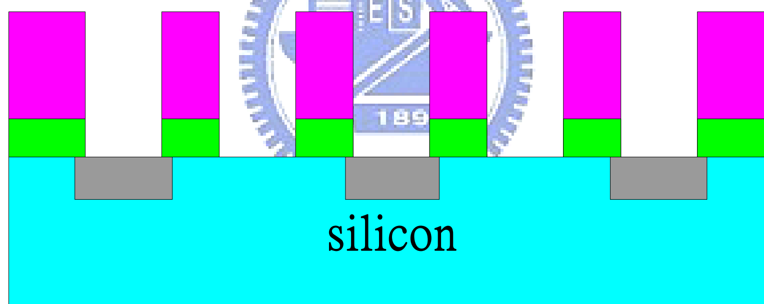

(g) mask II

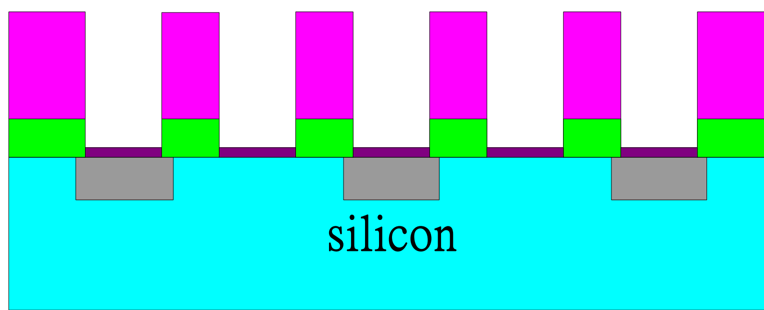

(h) dry oxidation

Figure 3-1 Experimental process

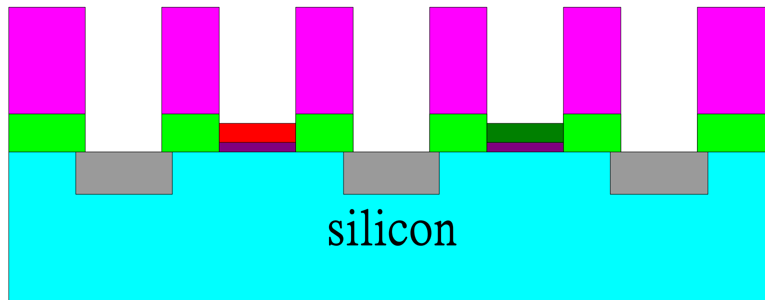

(i) sensing layers deposition and mask Ⅲ

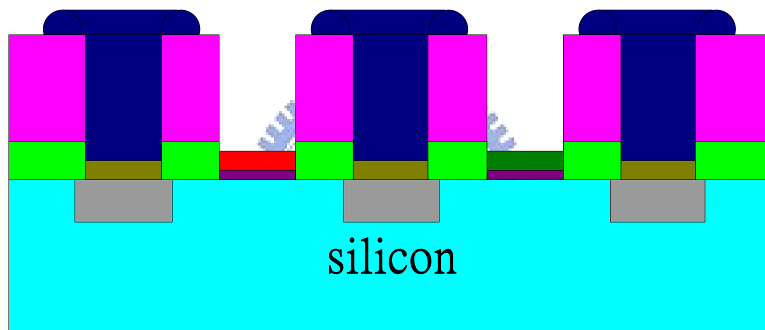

(j) Ti / Pt deposition and mask Ⅳ

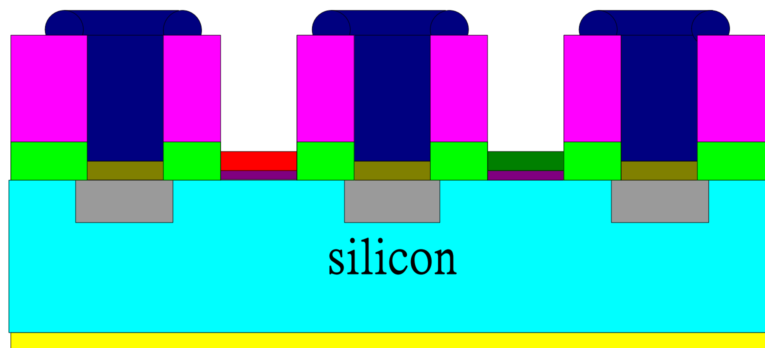

(k) backside Al deposition

Figure 3-1 Experimental process

Diameter (mm): 100+/-0.5
Type / Dopant : P / Boron
Orientation : <100>
Resistivity (ohm-cm):1-10
Thickness (μ m) ：505-545
Grade : Prime

Table 3-1 Specifications of wafers

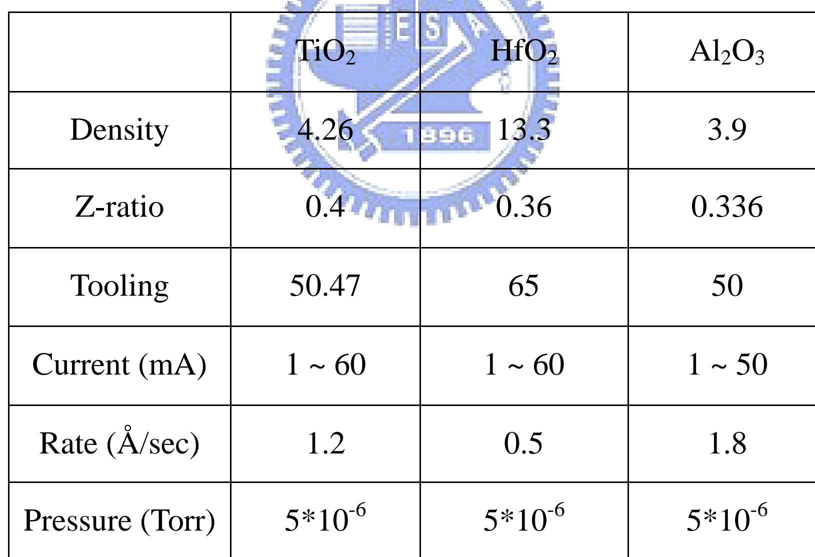

	TiO_2	HfO_2	Al_2O_3
Density	4.26	13.3	3.9
Z-ratio	0.4	0.36	0.336
Tooling	50.47	65	50
Current (mA)	1 ~ 60	1 ~ 60	1 ~ 50
Rate (Å/sec)	1.2	0.5	1.8
Pressure (Torr)	$5*10^{-6}$	$5*10^{-6}$	$5*10^{-6}$

E – gun

Table 3-2-a Parameters of sensing layers deposition with E – gun

parameters of HfO_2 sputter	parameters of ZrO_2 sputter
power : 200 W	power : 200 W
Ar / O_2 : 24 / 8 (sccm)	Ar / O_2 : 24 / 8 (sccm)
Density : 13.9	Density : 6.51
Acoustic impendance : 24.53	Acoustic impendance : 14.72
Tooling factor : 0.533	Tooling factor : 0.533
Rate : 0.01 Å / s	Rate : 0.01 Å / s
pre sputter 60W for 10 min	pre sputter 60W for 10 min
Pressure : 7.6×10^{-3}	Pressure : 7.6×10^{-3}

Sputter

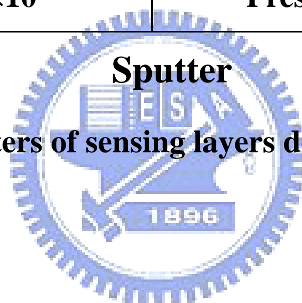

Table 3-2-b Parameters of sensing layers deposition with Sputter

parameters of LP-nitride deposition
NH_3 : 17 sccm
SiH_2Cl_2 : 85 sccm
1000 Å for 13 min
Temperature : 850 ℃
Pressure : 180 mT

LPCVD

Table 3-2-c Parameters of sensing layers deposition with LPCVD

HDP-RIE
Process pressure : 10 mTorr
flow rate of CHF_3 : 40 sccm
flow rate of Ar : 40 sccm
ICP power : 600 W
Bias power : 150 W
etch time of LP-nitride : 21 sec

Table 3-3 Recipe of HDP-RIE for LP-nitride

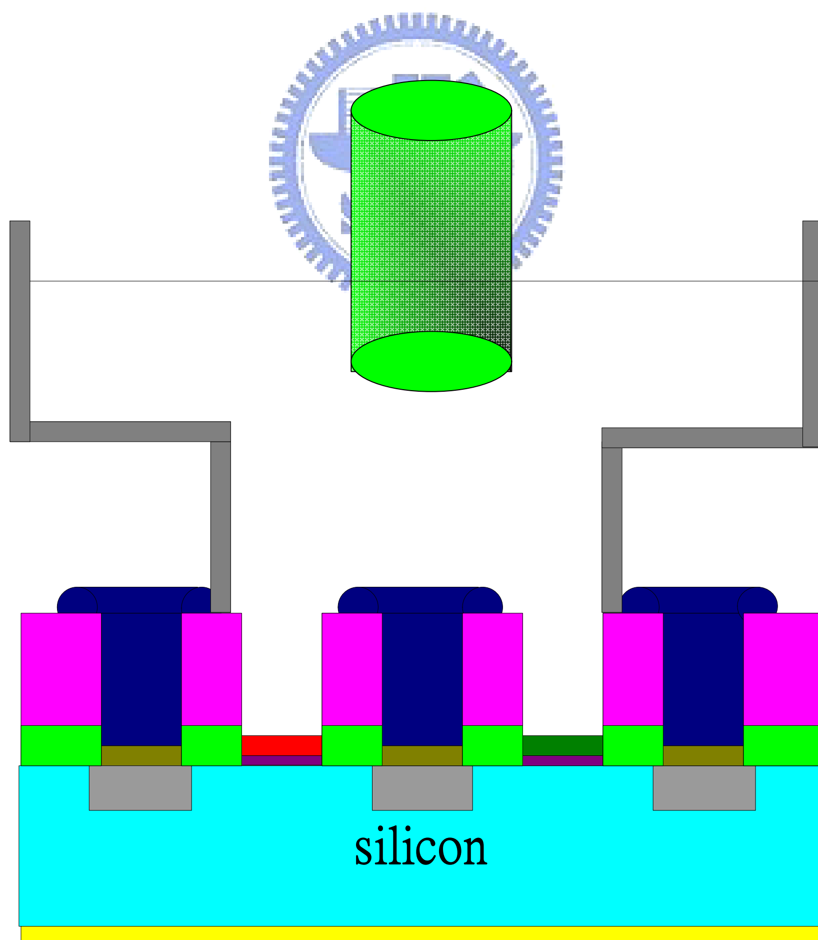

Figure 3-2 The system of measurement

sample	L	R		sample	L	R
#1	S-HfO_2	LP nitride		#7	S-ZrO_2	LP nitride
#2	E-HfO_2	LP nitride		#8	S-HfO_2	S-ZrO_2
#3	E-TiO_2	LP nitride		#9	S-HfO_2	E-Al_2O_3
#4	E-Al_2O_3	LP nitride		#10	E-TiO_2	S-ZrO_2
#5	E-HfO_2	S-HfO_2		#11	E-TiO_2	E-Al_2O_3
#6	E-HfO_2	E-TiO_2		#12	S-ZrO_2	E-Al_2O_3

Table 4-1 Table of composition of ISFET – ReFET pairs

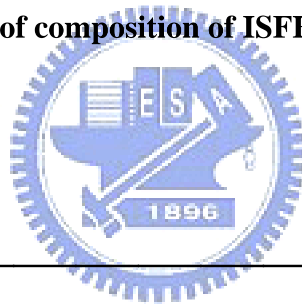

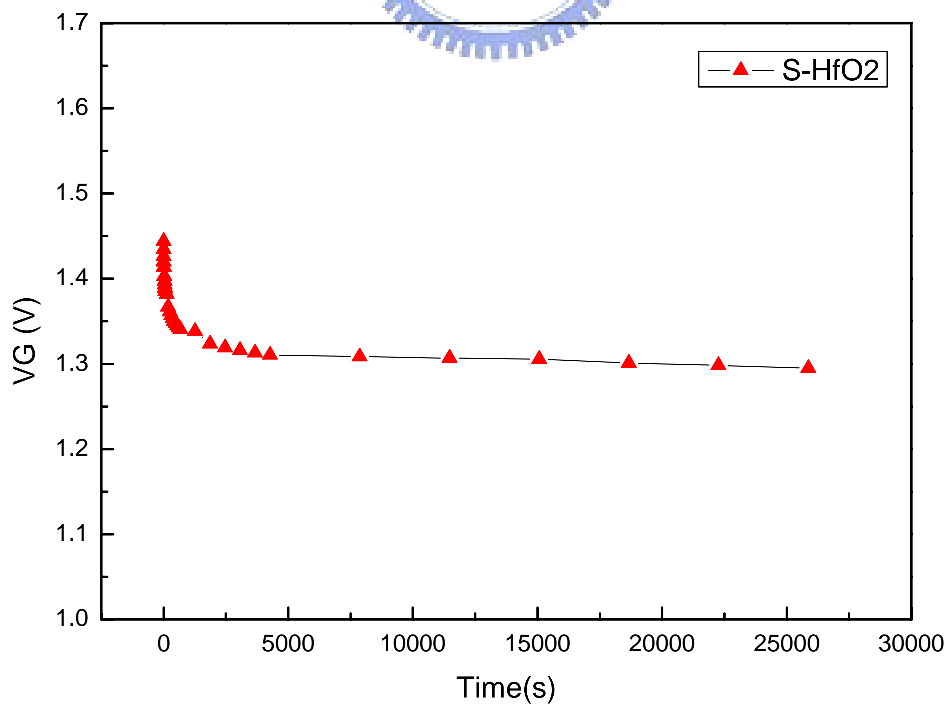

Figure 4-1-a drift characteristic of sputter HfO_2 (sample-1)

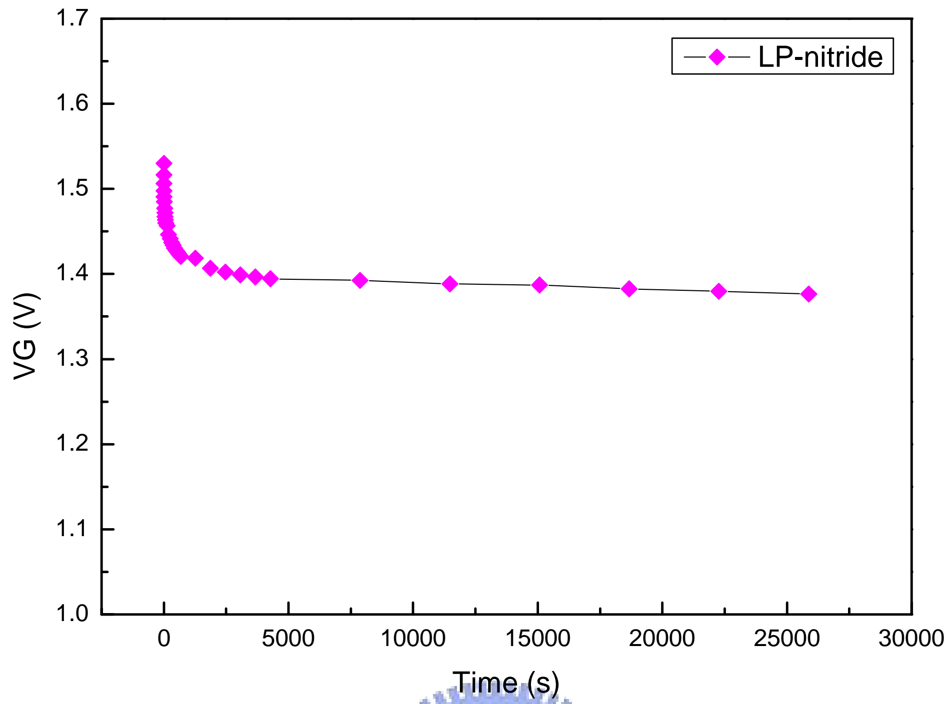

Figure 4-1-b drift characteristic of LP-nitride (sample-1)

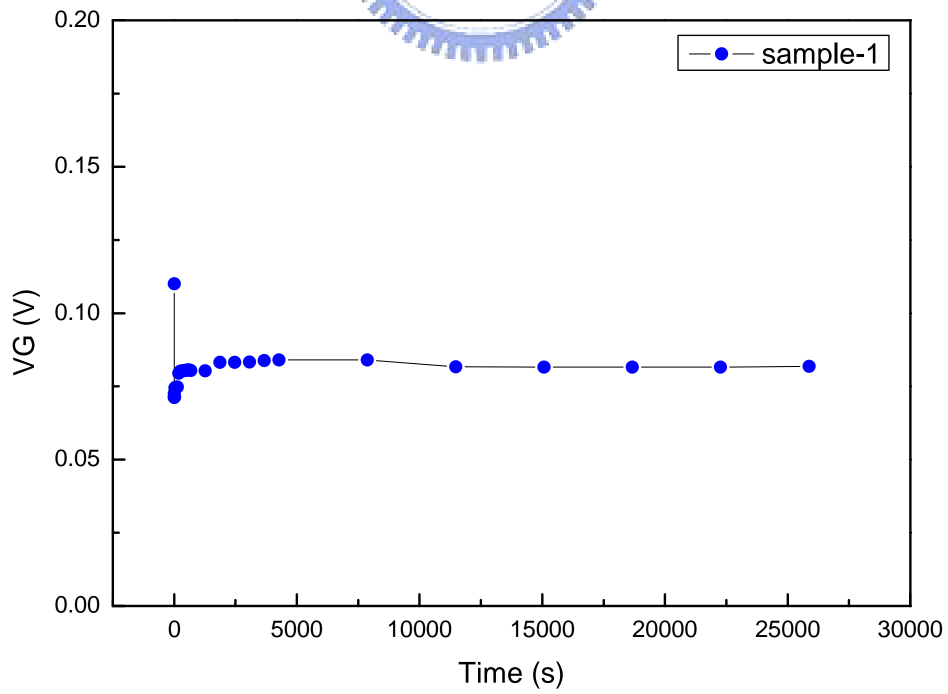

Figure 4-1-c drift characteristic of sample-1

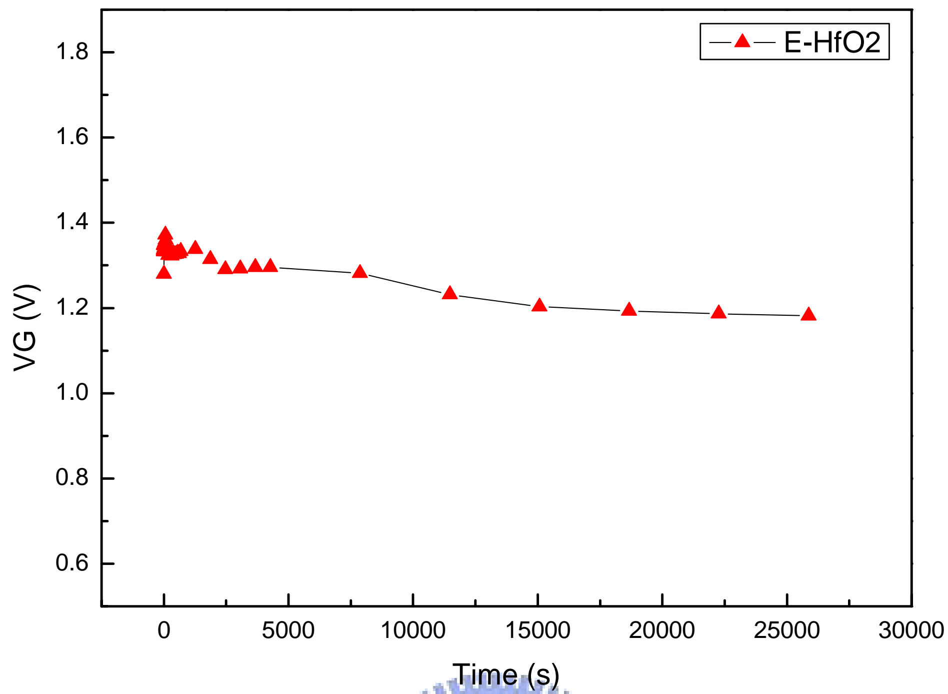

Figure 4-2-a drift characteristic of E-gun HfO_2 (sample-2)

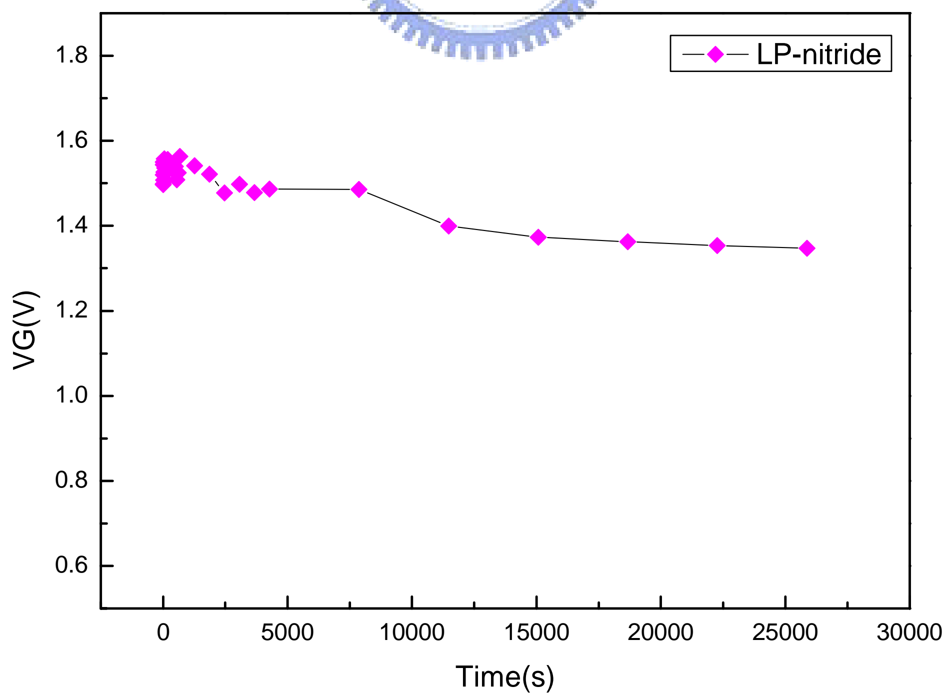

Figure 4-2-b drift characteristic of LP-nitride (sample-2)

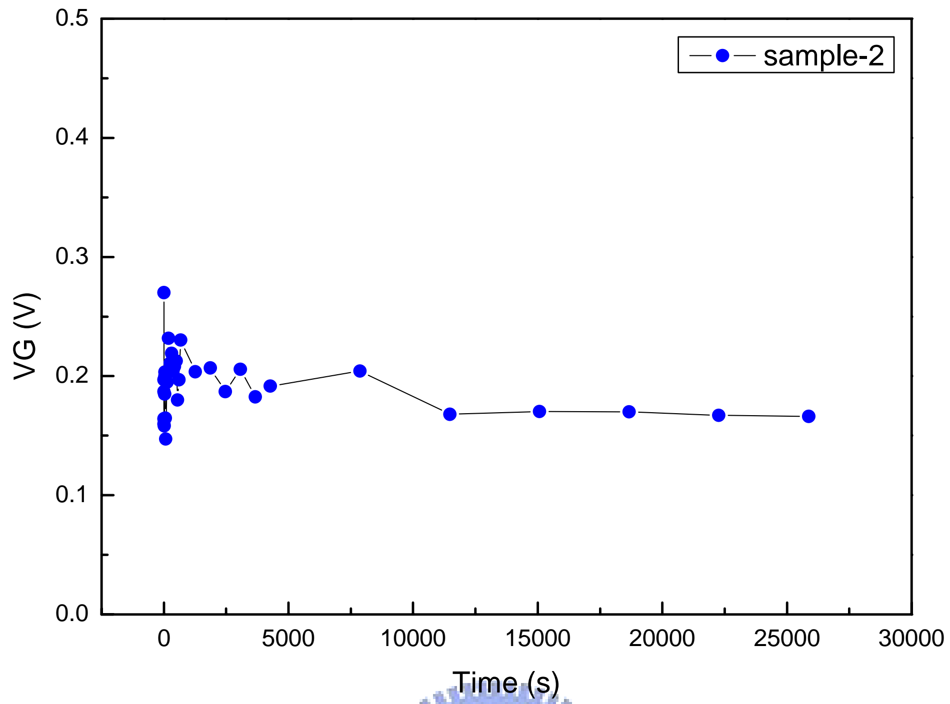

Figure 4-2-c drift characteristic of sample-2

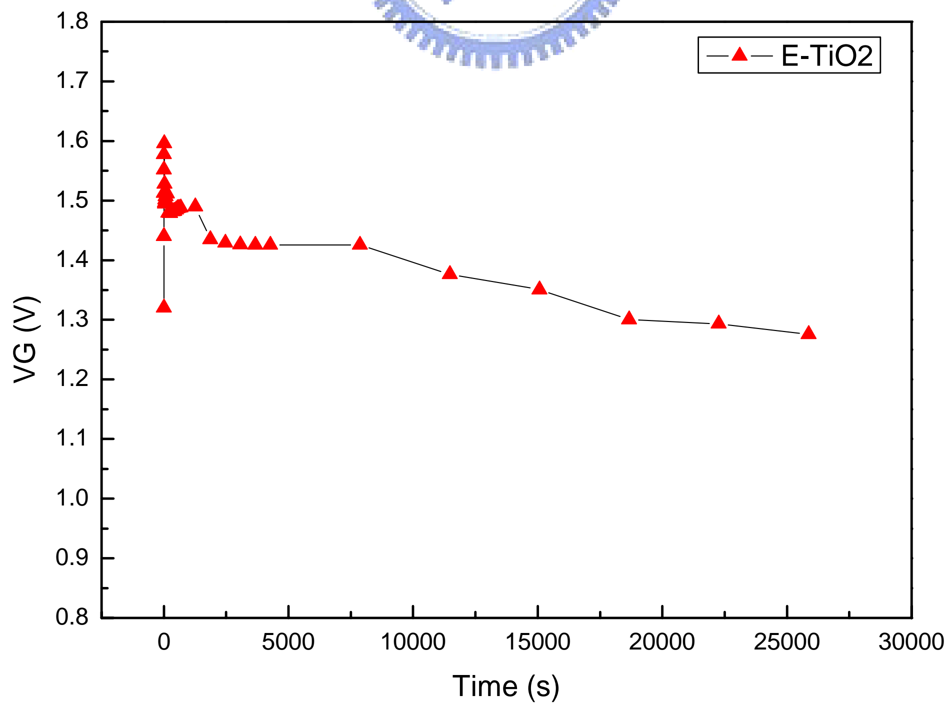

Figure 4-3-a drift characteristic of E-gun TiO_2 (sample-3)

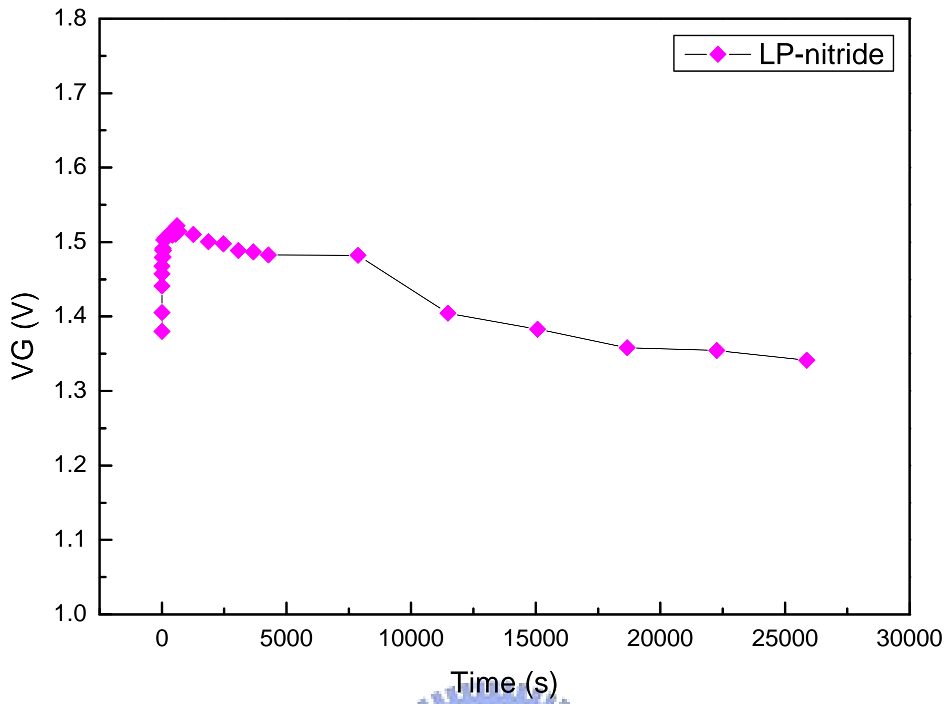

Figure 4-3-b drift characteristic of LP-nitride (sample-3)

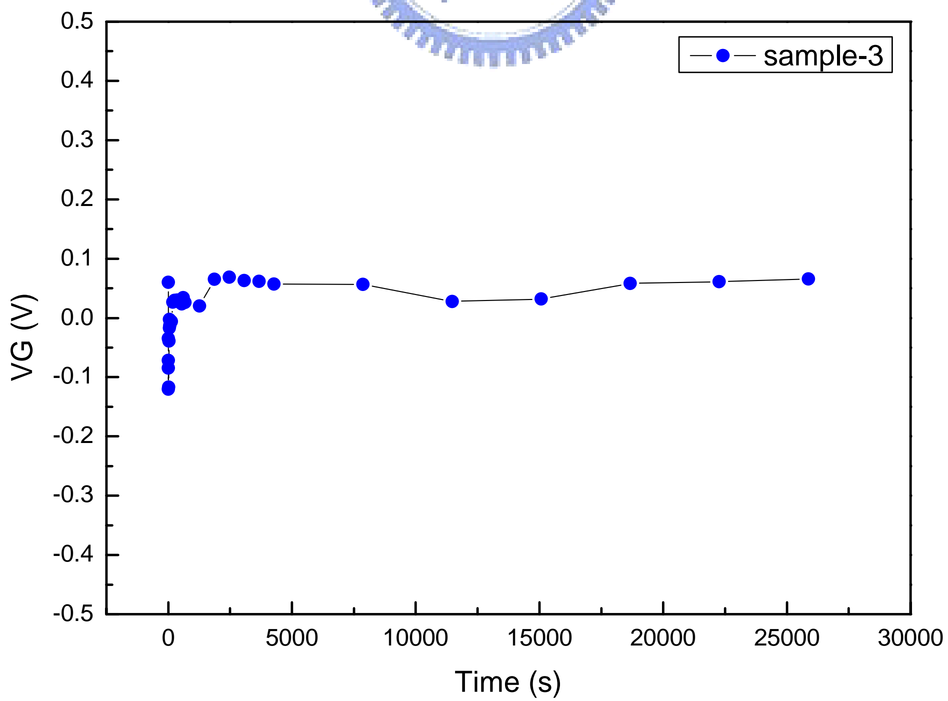

Figure 4-3-c drift characteristic of sample-3

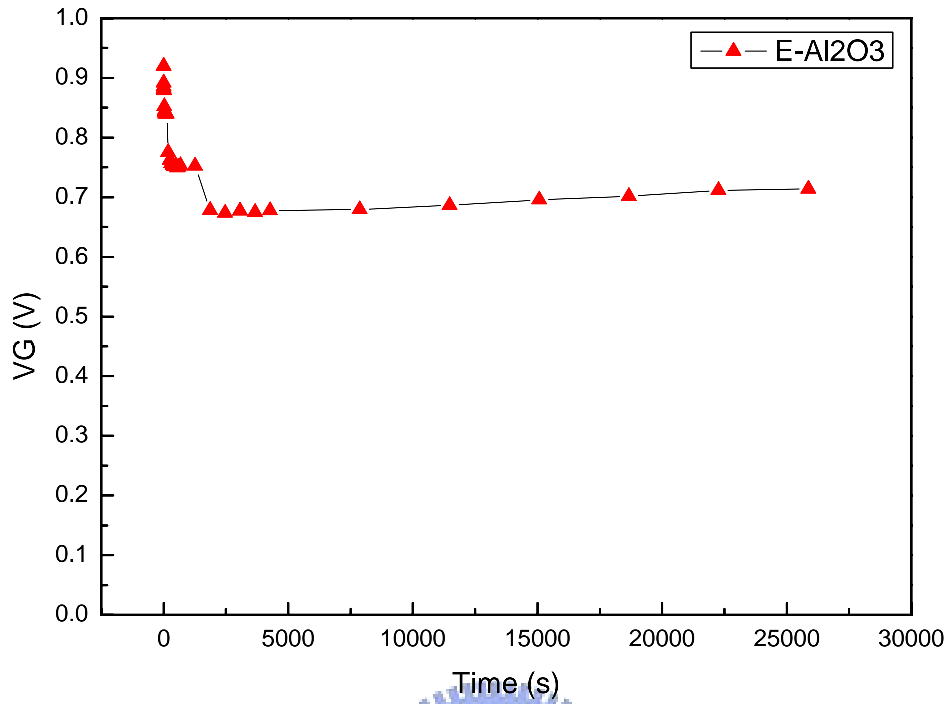

Figure 4-4-a drift characteristic of E-gun Al_2O_3 (sample-4)

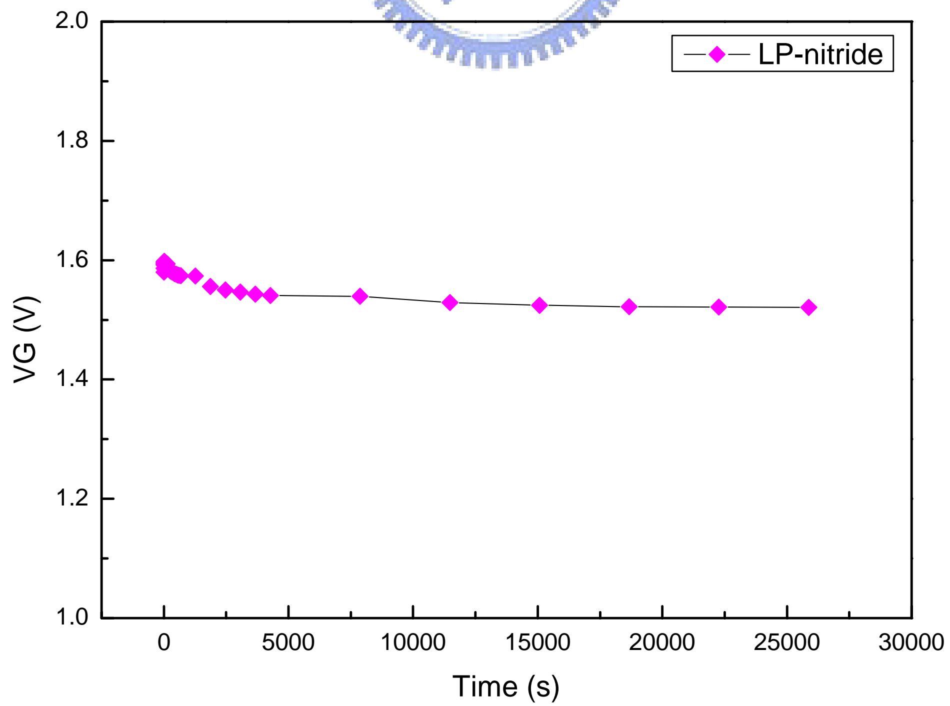

Figure 4-4-b drift characteristic of LP-nitride (sample-4)

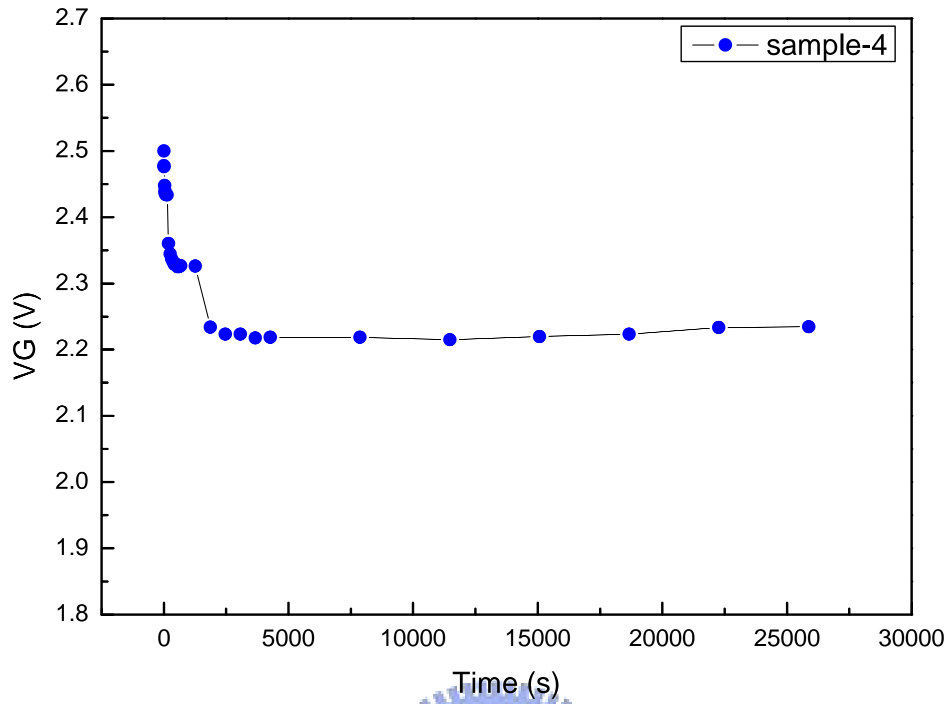

Figure 4-4-c drift characteristic of sample-4

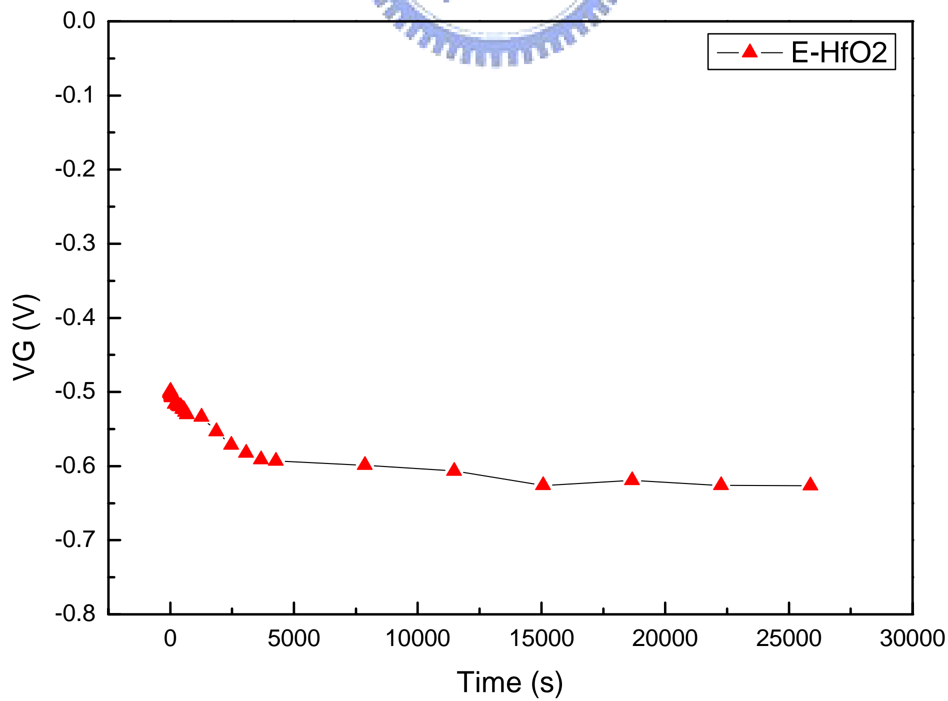

Figure 4-5-a drift characteristic of E-gun HfO_2 (sample-5)

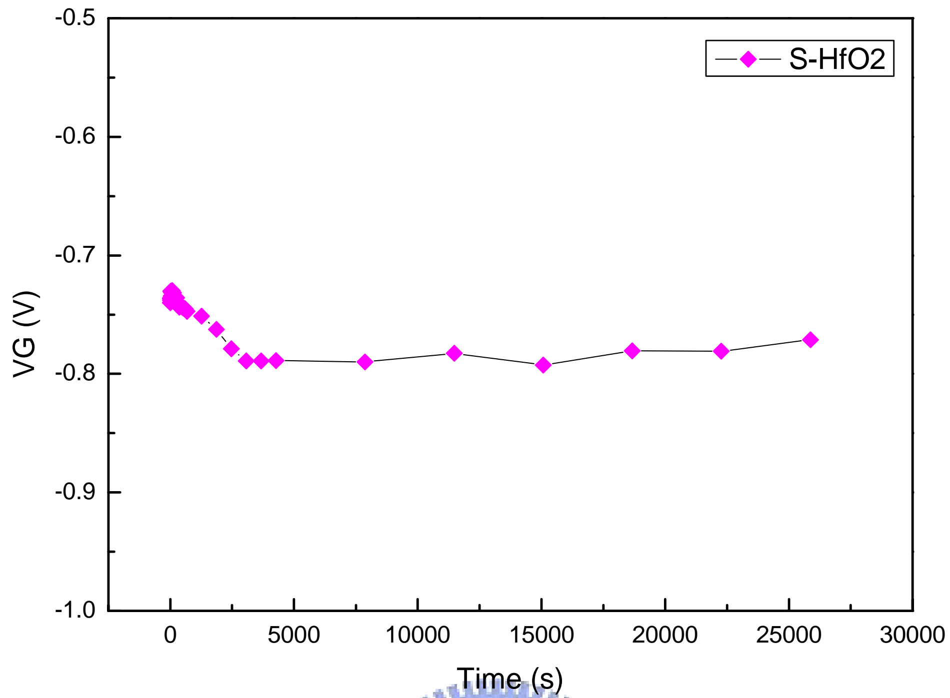

Figure 4-5-b drift characteristic of Sputter HfO_2 (sample-5)

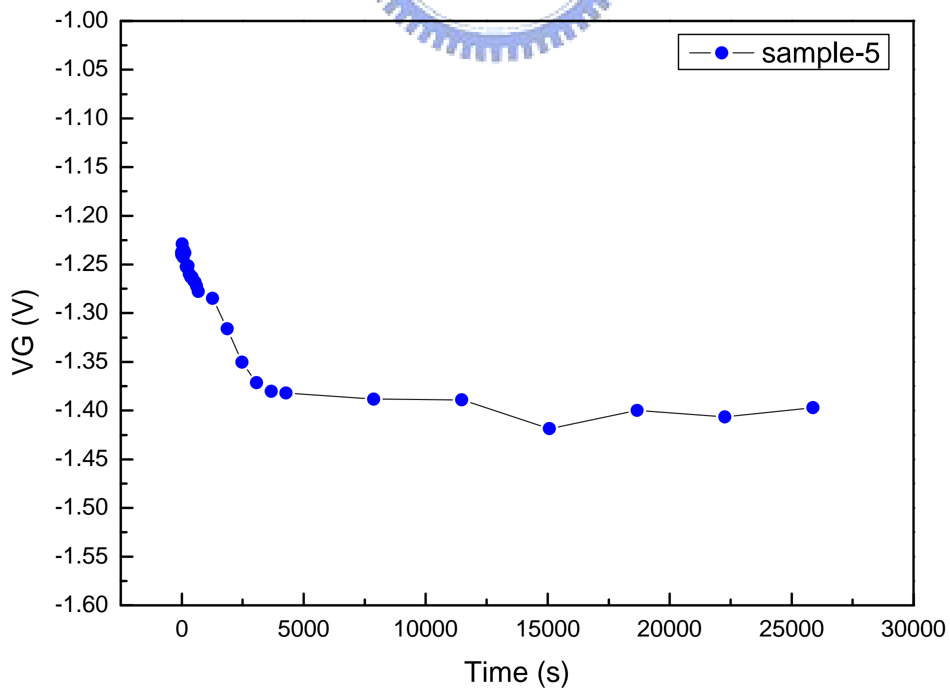

Figure 4-5-c drift characteristic of sample-5

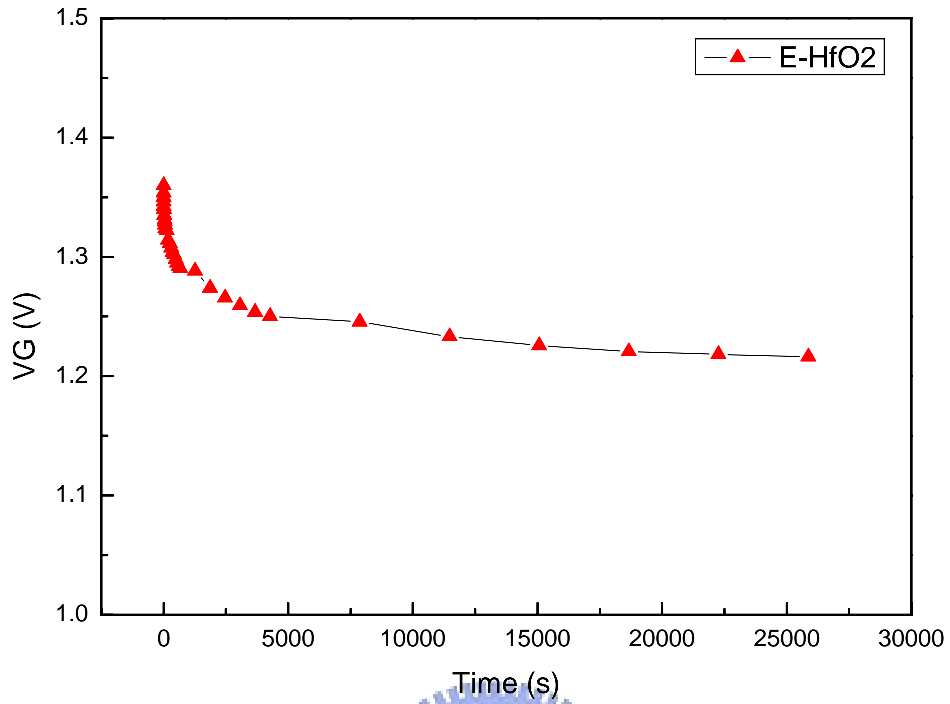

Figure 4-6-a drift characteristic of E-gun HfO_2 (sample-6)

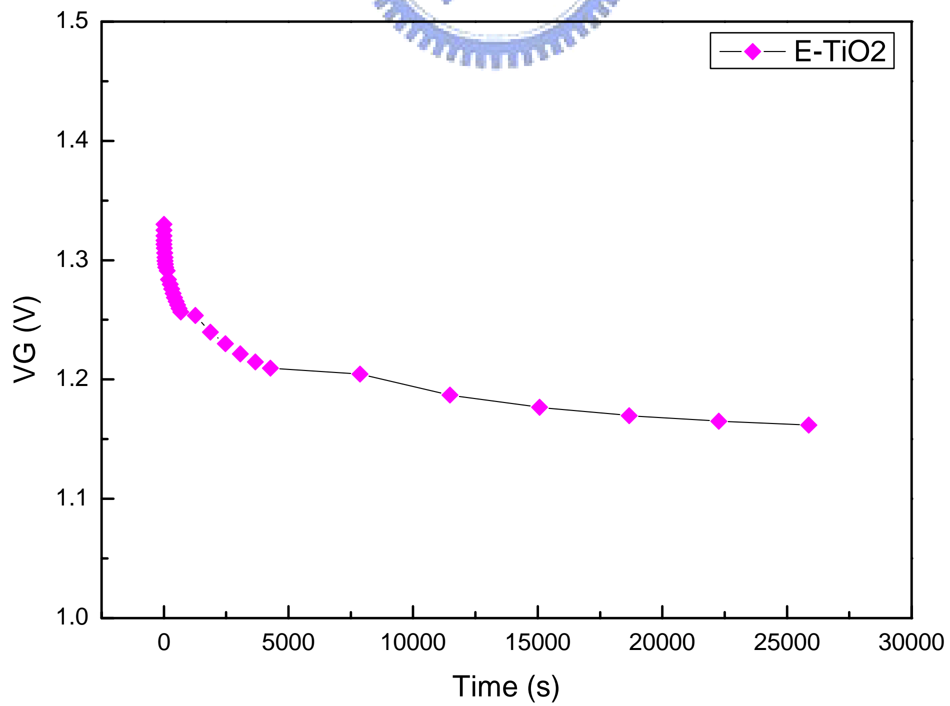

Figure 4-6-b drift characteristic of E-gun TiO_2 (sample-6)

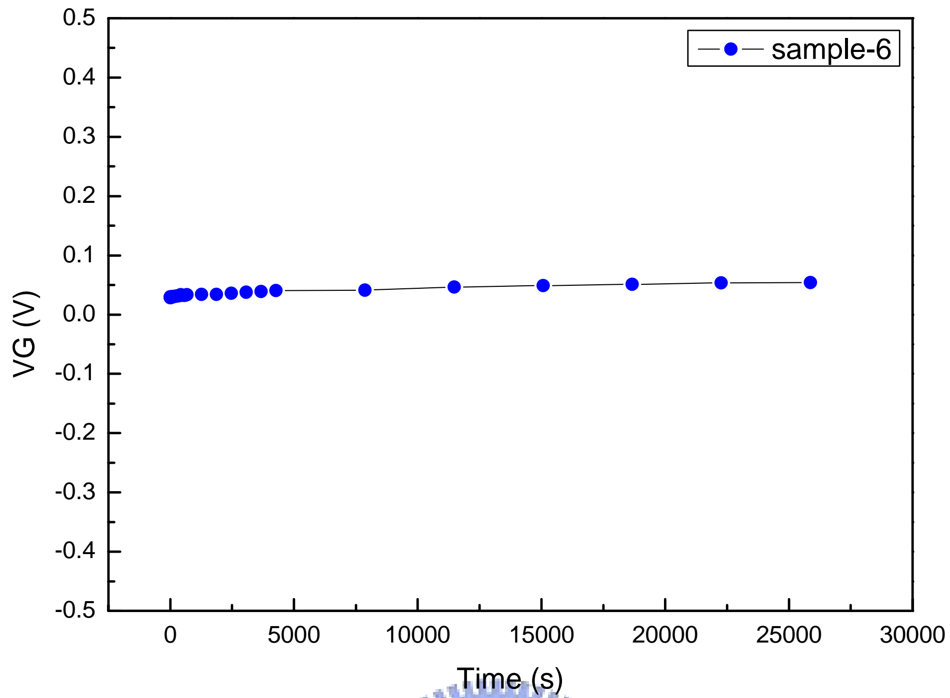

Figure 4-6-c drift characteristic of sample-6

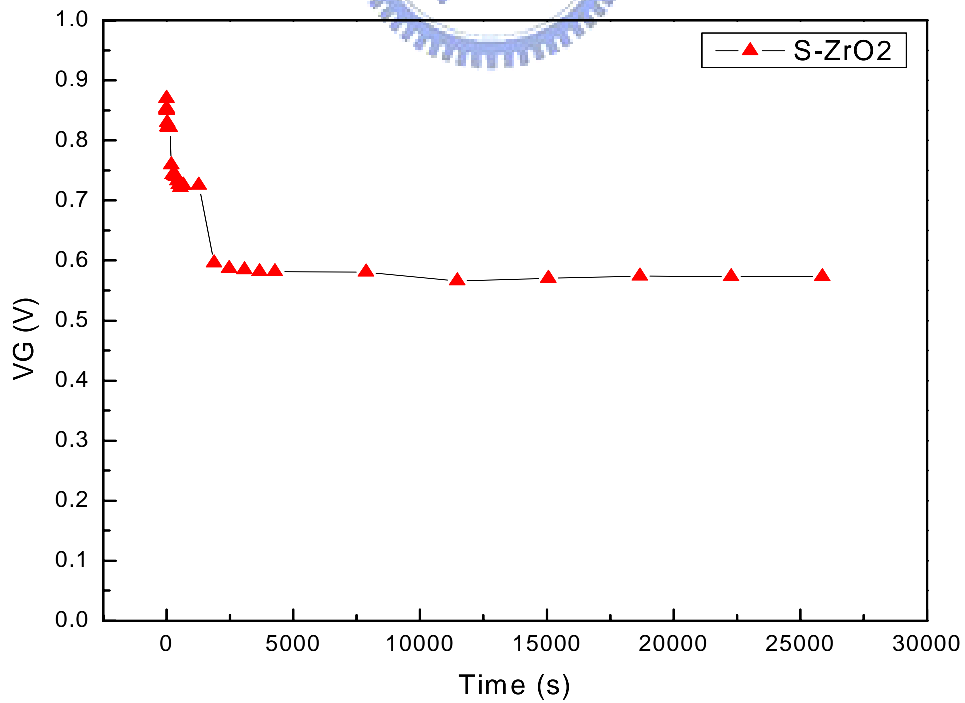

Figure 4-7-a drift characteristic of Sputter ZrO_2 (sample-7)

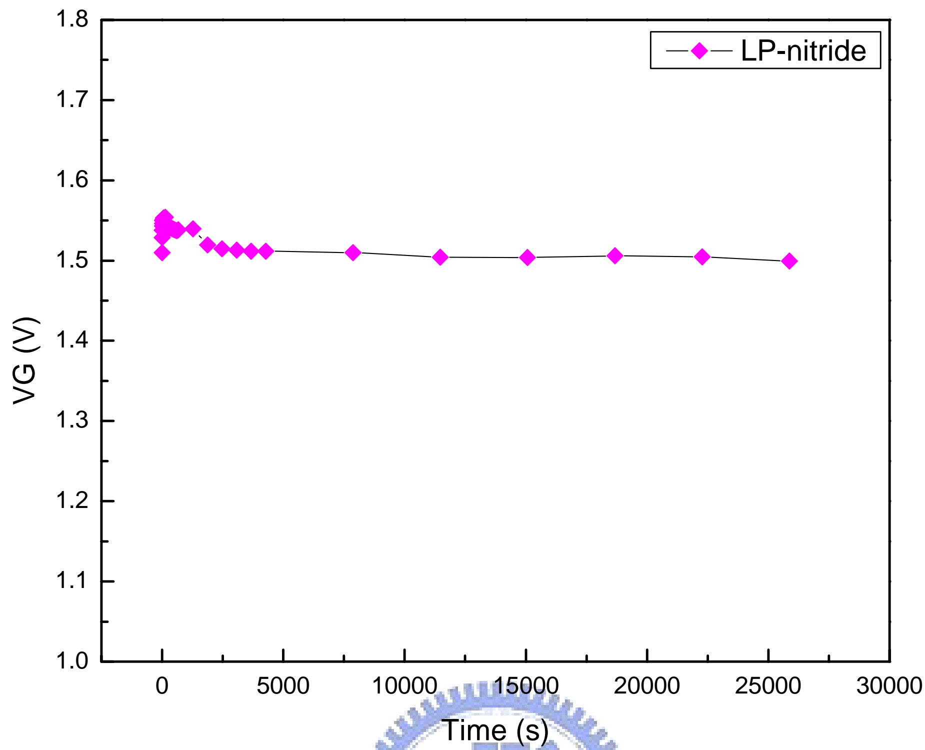

Figure 4-7-b drift characteristic of LP-nitride (sample-7)

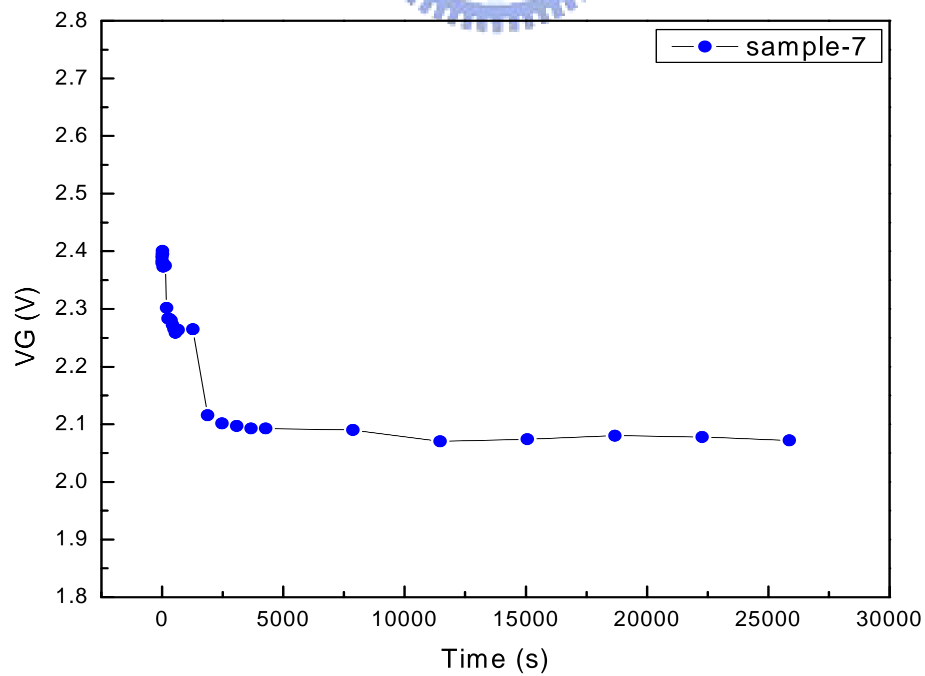

Figure 4-7-c drift characteristic of sample-7

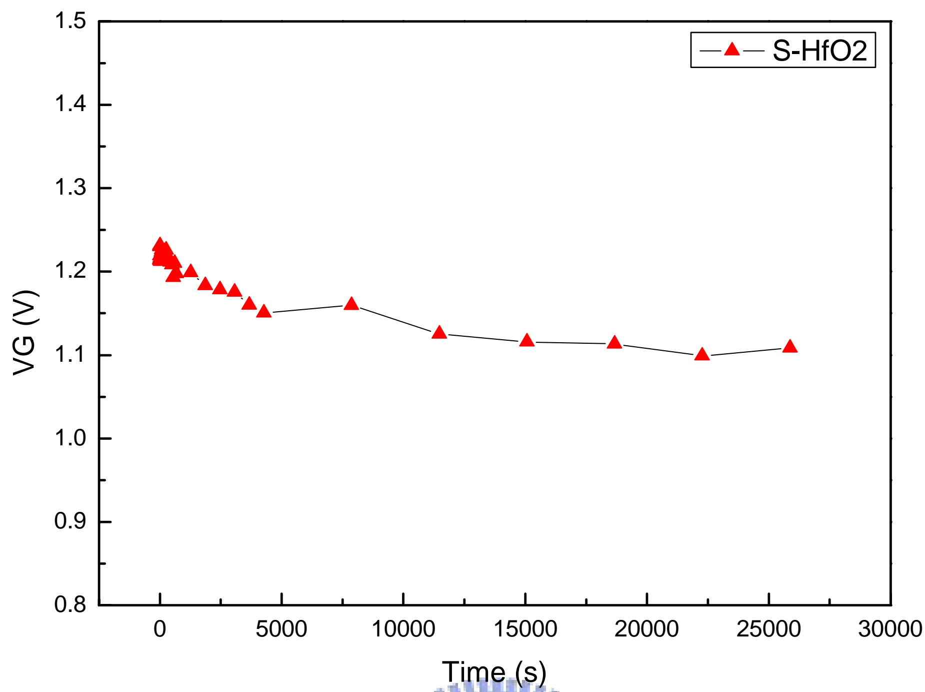

Figure 4-8-a drift characteristic of Sputter HfO_2 (sample-8)

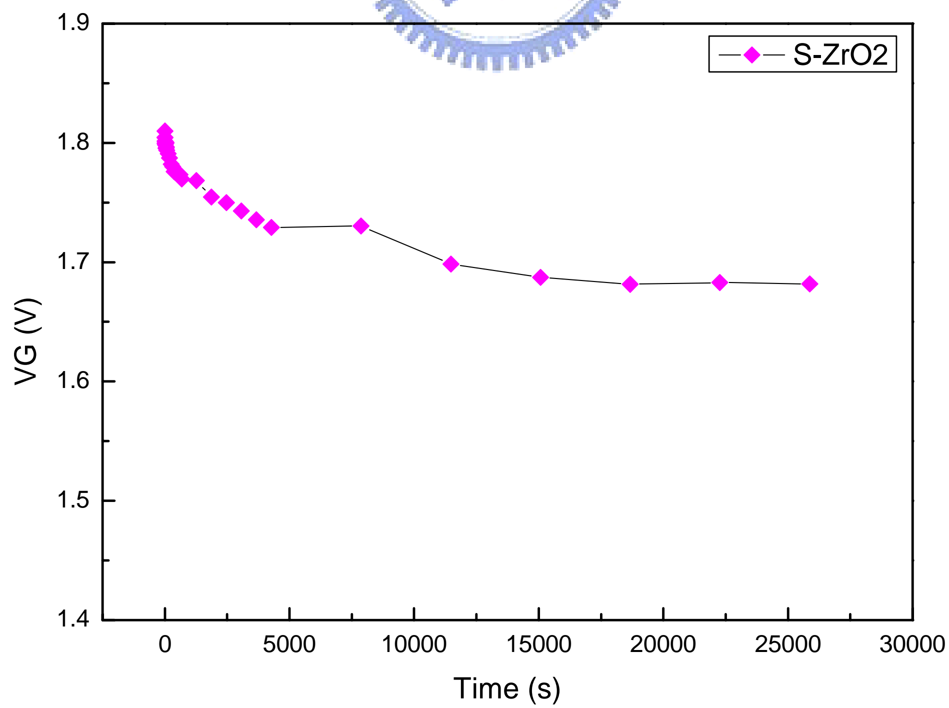

Figure 4-8-b drift characteristic of Sputter ZrO_2 (sample-8)

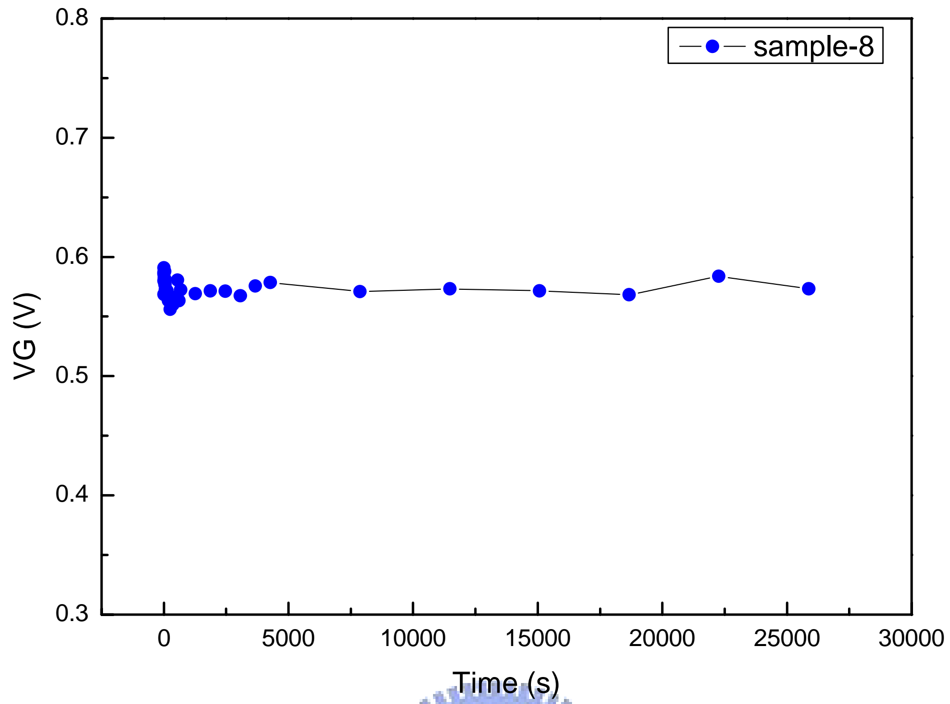

Figure 4-8-c drift characteristic of sample-8

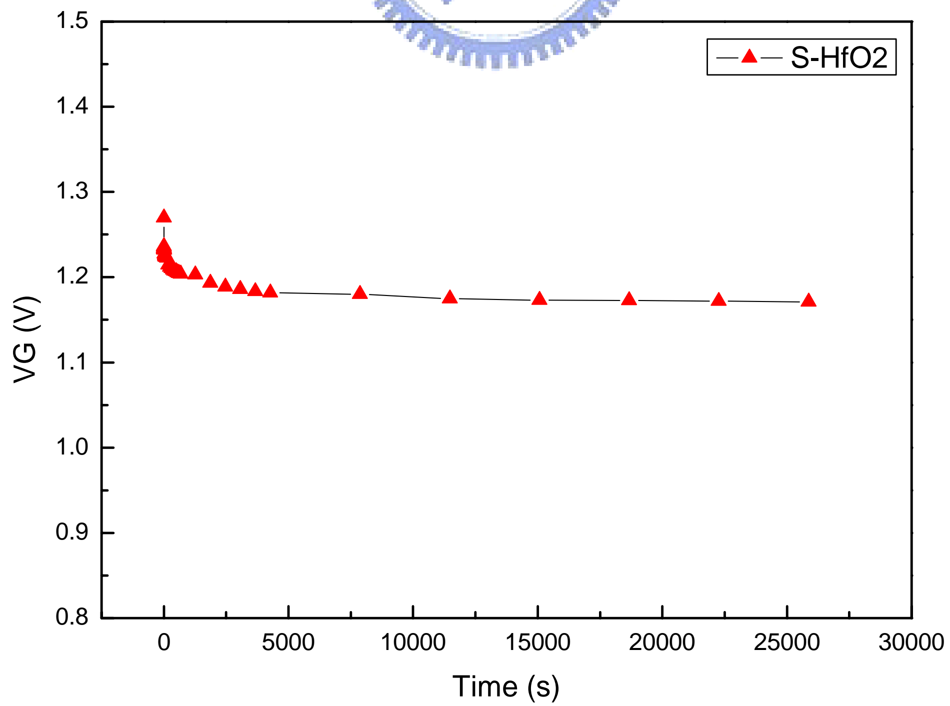

Figure 4-9-a drift characteristic of Sputter HfO_2 (sample-9)

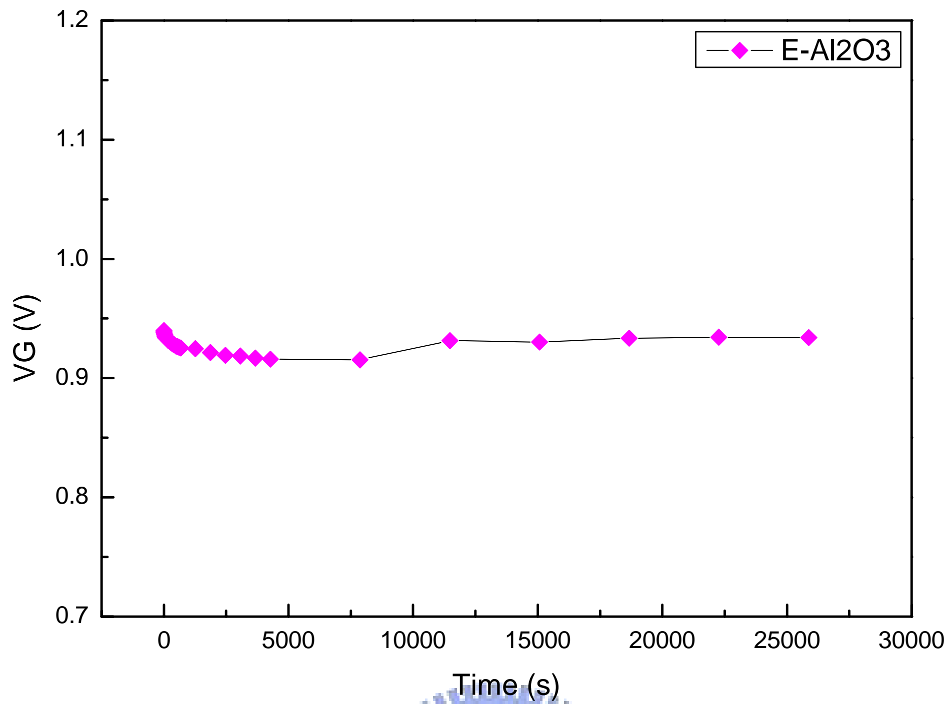

Figure 4-9-b drift characteristic of E-gun Al_2O_3 (sample-9)

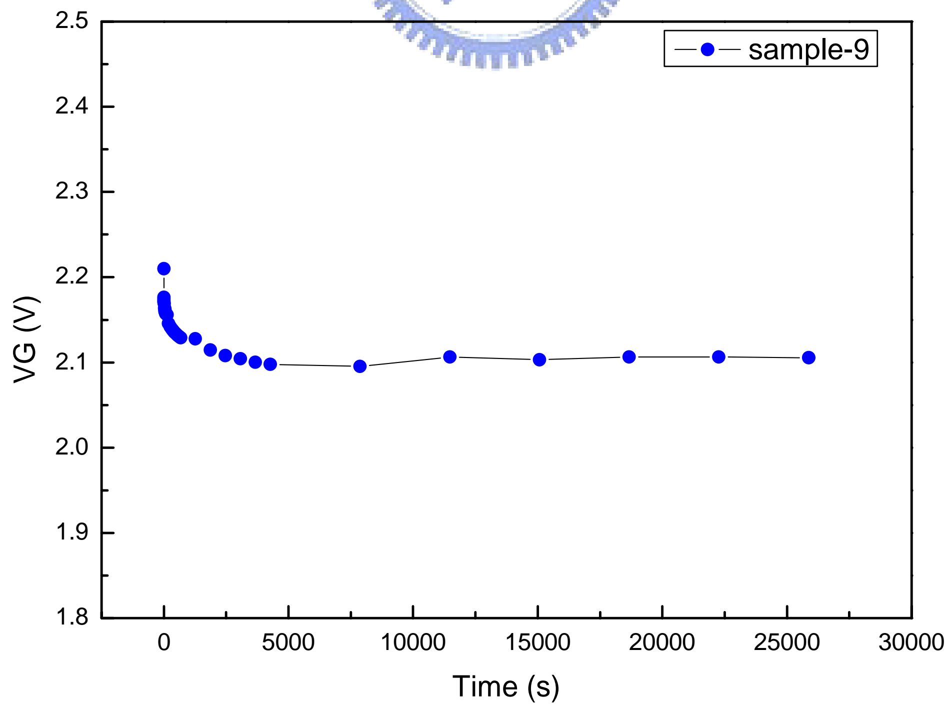

Figure 4-9-c drift characteristic of sample-9

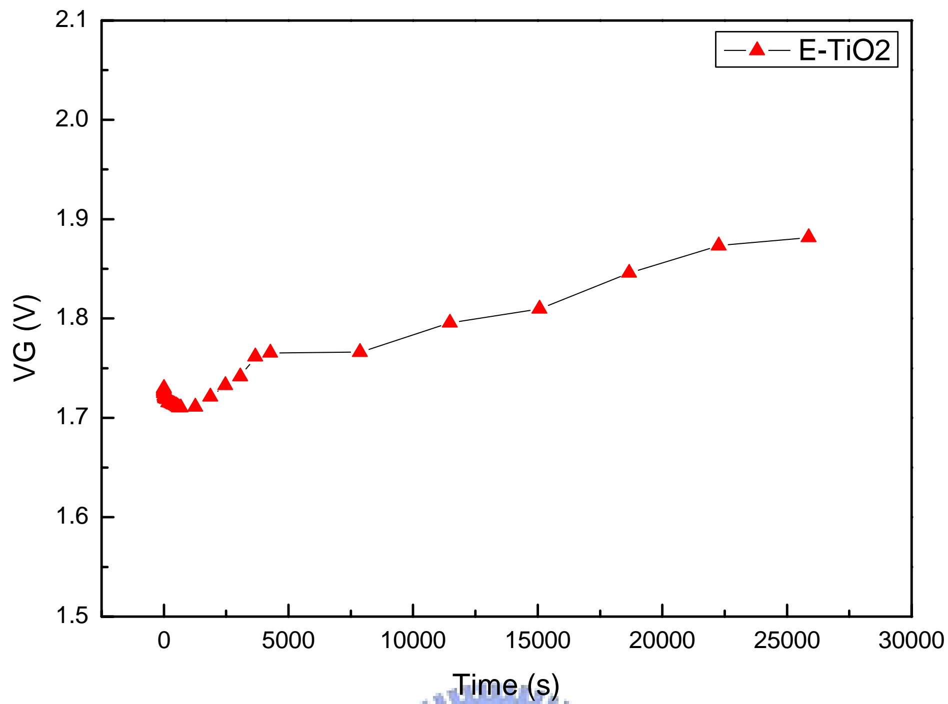

Figure 4-10-a drift characteristic of E-gun TiO_2 (sample-10)

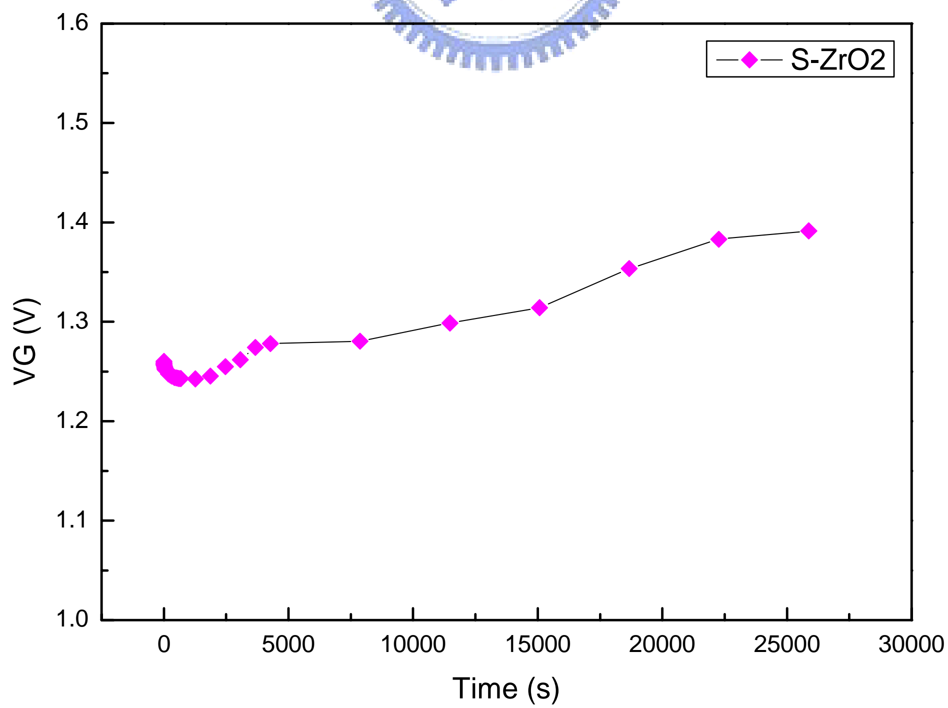

Figure 4-10-b drift characteristic of Sputter ZrO_2 (sample-10)

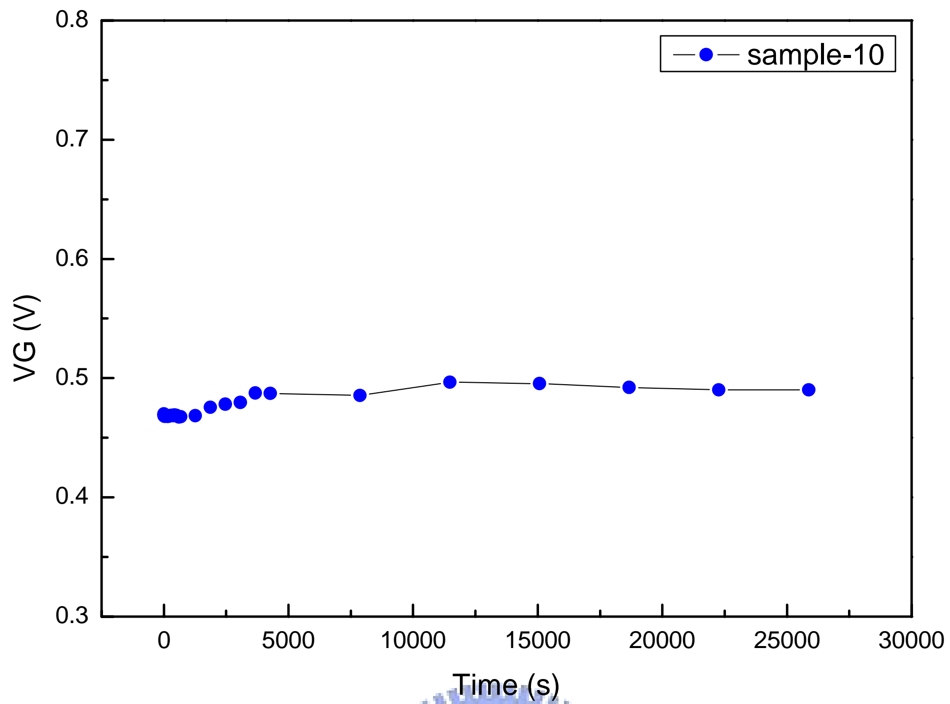

Figure 4-10-c drift characteristic of sample-10

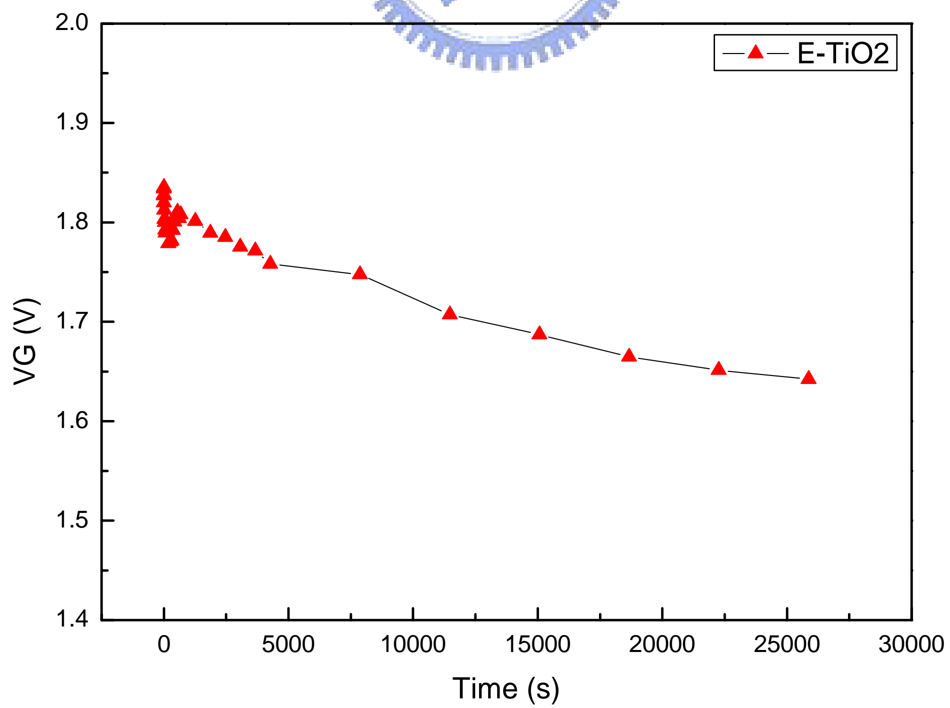

Figure 4-11-a drift characteristic of E-gun TiO_2 (sample-11)

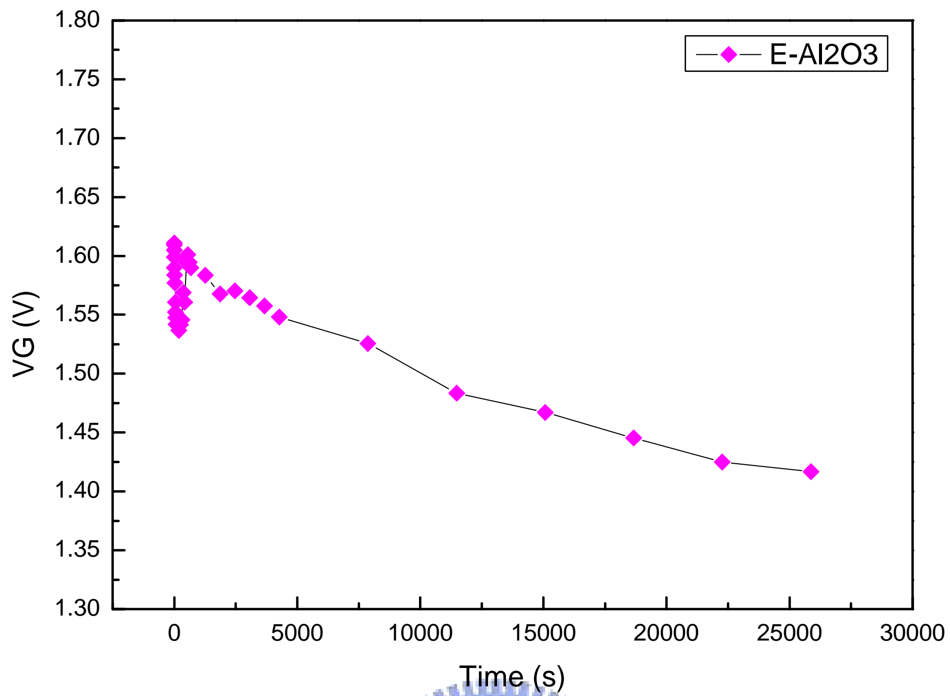

Figure 4-11-b drift characteristic of E-gun Al_2O_3 (sample-11)

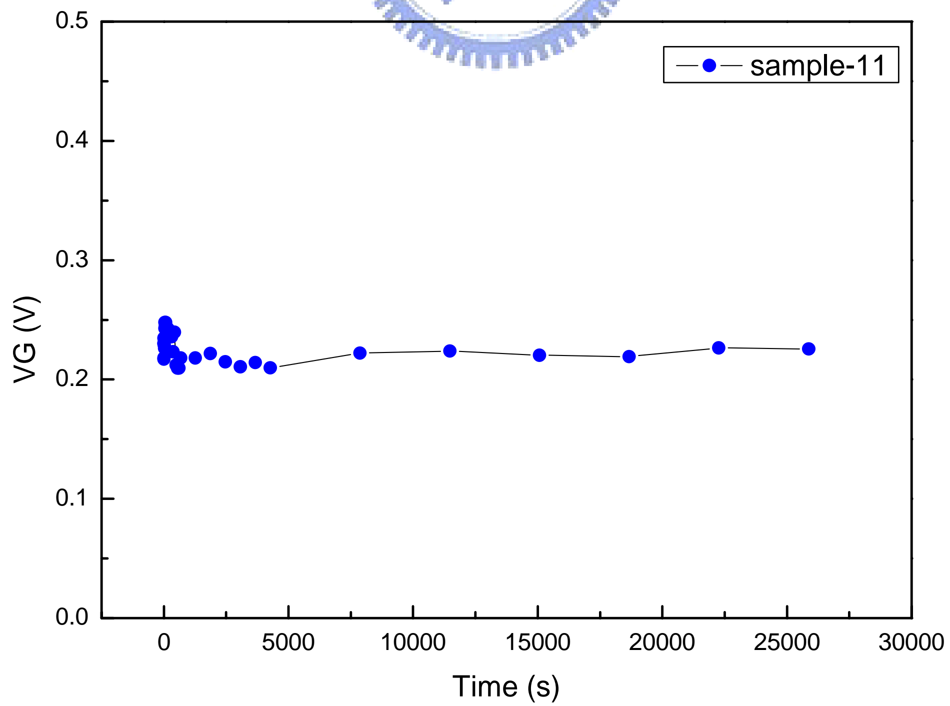

Figure 4-11-c drift characteristic of sample-11

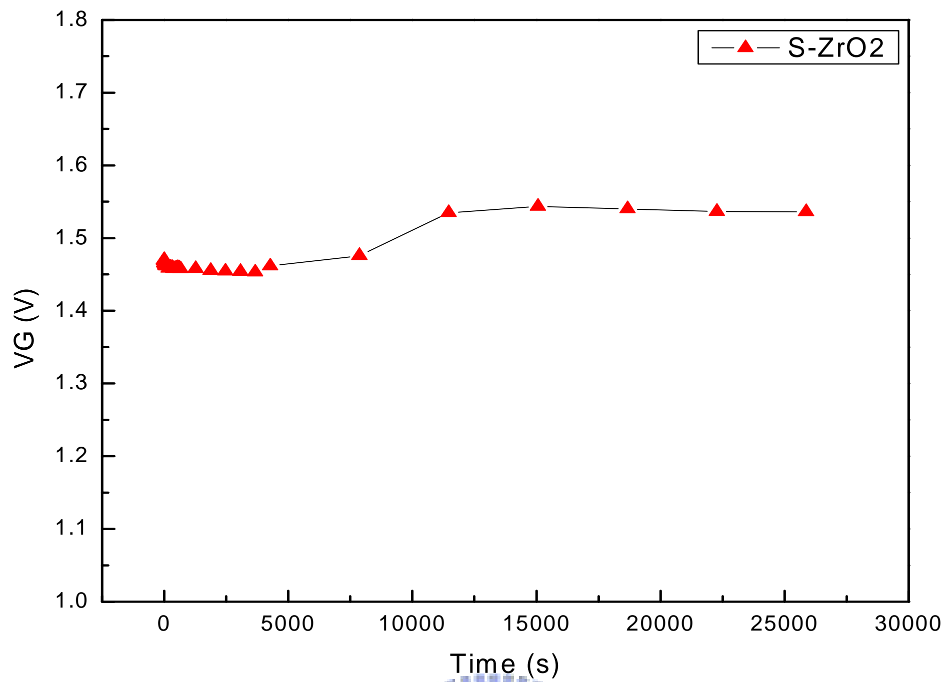

Figure 4-12-a drift characteristic of Sputter ZrO_2 (sample-12)

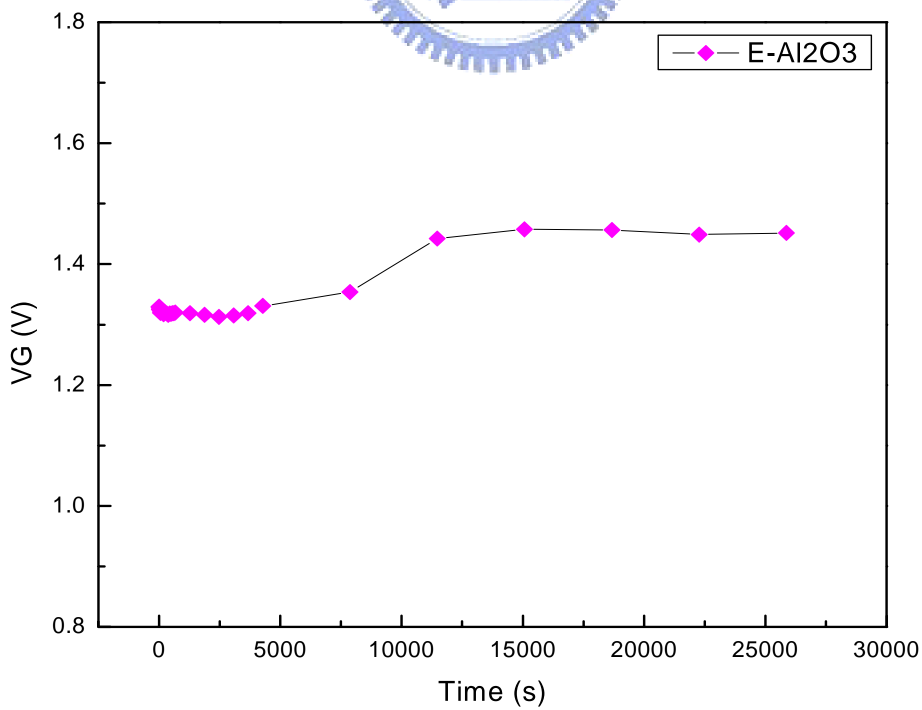

Figure 4-12-b drift characteristic of E-gun Al_2O_3 (sample-12)

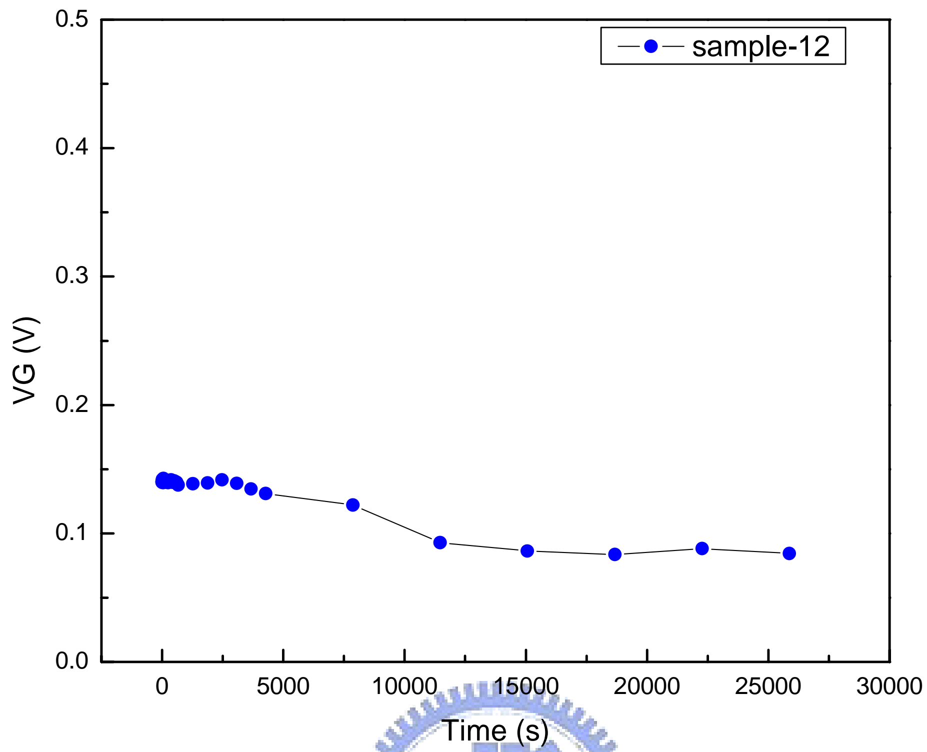

Figure 4-12-c drift characteristic of sample-12

	Type	Drift (mv/hr)	Difference	Correction(%)
	L/R	(10000 s ~)		
Sample-1	**S-HfO_2**	2.85369	0.190548	**93.32**
	nitride	3.04423	0.190548	**93.74**
Sample-2	**E-HfO_2**	16.1036	3.74291	**76.76**
	nitride	19.8465	3.74291	**81.14**
Sample-3	**E-TiO_2**	27.3981	5.896106	**78.48**
	nitride	21.5025	5.8956	**72.58**
Sample-4	**E-Al_2O_3**	6.912363	4.090433	**40.82**
	nitride	2.82193	4.090433	**-44.95**
Sample-5	**E-HfO_2**	5.18336	1.90321	**63.28**
	S-HfO_2	3.280151	1.90321	**41.98**
Sample-6	**E-HfO_2**	5.01777	2.29111	**54.34**
	E-TiO_2	7.30888	2.291115	**68.65**
Sample-7	**S-ZrO_2**	0.226389	1.4155	**-525.25**
	nitride	1.64234	1.4155	**13.81**
Sample-8	**S-HfO_2**	6.96181	0.22707	**96.74**
	S-ZrO_2	6.73497	0.22707	**96.63**

Table 4-2 The drift after 10000 s and the relative correction coefficient

	Type	Drift (mv/hr)	Difference	Correction(%)
	L/R	(10000 s ~)		
Sample-9	**S-HfO_2**	1.27486	0.838866	**34.2**
	E-Al_2O_3	2.11327	0.838866	**60.305**
Sample-10	**E-TiO_2**	22.22541	0.431	**98.06**
	S-ZrO_2	22.65891	0.431	**98.1**
Sample-11	**E-TiO_2**	18.4696	0.54397	**97.05**
	E-Al_2O_3	19.014	0.54397	**97.14**
Sample-12	**S-ZrO_2**	5.744575	4.61626	**19.64**
	E-Al_2O_3	10.36015	4.61626	**55.44**

Table 4-2 The drift after 10000 s and the relative correction coefficient